A circadian clock in the sinus node mediates day-night rhythms in Hcn4 and heart rate

Alicia D'souza, Yanwen Wang, Cali Anderson, Annalisa Bucchi, Mirko Baruscotti, Servé Olieslagers, Pietro Mesirca, Anne Berit Johnsen, Svetlana Mastitskaya, Haibo Ni, et al.

A circadian clock in the sinus node mediates day-night rhythms in *Hcn4* and heart rate

Running title: Circadian rhythms in *Hcn4* and heart rate

Alicia D'Souza BSc, PhD[1*]; Yanwen Wang BSc, PhD[1*]; Cali Anderson MRes[1]; Annalisa Bucchi BSc, PhD[2]; Mirko Barsucotti BSc, PhD[2]; Servé Olieslagers MSc[3]; Pietro Mesirca BSc, PhD[4]; Anne Berit Johnsen BSc, PhD[5]; Svetlana Mastitskaya BSc, PhD[6]; Haibo Ni BSc, PhD[1]; Yu Zhang BSc, PhD[1]; Nicholas Black BmBCh[1]; Charlotte Cox MSc[1]; Sven Wegner BmBCh , PhD[1]; Beatriz Bano-Otalora BSc, PhD[1]; Cheryl Petit MSc[1]; Eleanor Gill BSc, PhD[1]; Sunil Jit Logantha BSc, PhD[1]; Halina Dobrzynski BSc, PhD[1]; Nick Ashton BSc, PhD[1]; George Hart BmBCh, PhD [1]; Rai Zhang BSc, PhD[7]; Henggui Zhang BSc, PhD[1]; Elizabeth J Cartwright BSc, PhD[1]; Ulrik Wisloff BSc, PhD[5]; Matteo E. Mangoni BSc, PhD[4]; Paula Da Costa Martins BSc, PhD[3]; Hugh D. Piggins BSc, PhD[7]; Dario DiFrancesco BSc, PhD[2]; Mark R. Boyett BSc, PhD, FRSB, FRCP[8]

[1]University of Manchester, Manchester, UK. [2]University of Milan, Milan, Italy. [3]Maastricht University, Maastricht, Netherlands. [4]CNRS, Montpellier, France. [5]Norwegian University of Science and Technology, Trondheim, Norway. [6]University College London, London, UK. [7]University of Bristol, Bristol, UK. [8]University of Copenhagen, Copenhagen, Denmark

*Equal contribution

Corresponding author: Alicia D'Souza; Division of Cardiovascular Sciences, University of Manchester, 46 Grafton Street, Manchester M13 9NT, UK

Email: alicia.dsouza@manchester.ac.uk

No conflicts to disclose

5,244 words

ABSTRACT

Background: Heart rate follows a diurnal variation and slow heart rhythms occur primarily at night.

Objective: The lower heart rate during sleep is assumed to be neural in origin but here we tested whether a day-night difference in intrinsic pacemaking is involved.

Methods: *In vivo* and *in vitro* ECG recordings, vagotomy, transgenics, quantitative polymerase chain reaction, western blotting, immunohistochemistry, patch clamp, reporter bioluminescence recordings and chromatin immunoprecipitation were used.

Results: The day-night difference in the average heart rate of mice was independent of fluctuations in average locomotor activity and persisted under pharmacological, surgical and transgenic interruption of autonomic input to the heart. Spontaneous beating rate of isolated (i.e. denervated) sinus node (SN) preparations exhibited a day-night rhythm concomitant with rhythmic mRNA expression of ion channels including HCN4. *In vitro* studies demonstrated 24 h rhythms in the human HCN4 promoter and the corresponding funny current. The day-night heart rate difference in mice was abolished by HCN block both *in vivo* and in the isolated SN. Rhythmic expression of canonical circadian clock factors, e.g. *Bmal1* and *Cry*, were identified in the SN and disruption of the local clock (by cardiac-specific knockout of *Bmal1*) abolished the day-night difference in *Hcn4* and intrinsic heart rate. Chromatin immunoprecipitation revealed specific BMAL1 binding sites on *Hcn4*, linking the local clock with intrinsic rate control.

Conclusion: The circadian variation in heart rate involves SN local clock-dependent *Hcn4* rhythmicity. Data reveal a novel regulator of heart rate and mechanistic insight into bradycardia during sleep.

Key words: Sinus node; Pacemaking; Circadian rhythm; Nocturnal bradycardia; Vagus nerve

INTRODUCTION

In humans, the resting heart rate exhibits diurnal rhythms and is higher during the day when we are awake.[1] The heart is therefore primed, anticipating the increase in demand during the awake period. Conversely, slow heart rhythms primarily occur at night during the sleep period.[1] The same occurs in the nocturnal rodent, but in reverse.[1]

For ~90 years, the day-night difference in heart rate *in vivo* in humans has been attributed to the autonomic nervous system[2] and primarily high vagal tone during sleep.[3] This is in large part based on heart rate variability (HRV) as a surrogate measure of autonomic tone.[3] However, from biophysical analysis of HRV we have previously demonstrated an exponential-like relationship between HRV and heart rate, and changes in HRV observed in humans and animal models are mainly attributable to the accompanying changes in heart rate.[4, 5] The involvement of the autonomic nervous system in the circadian rhythm in heart rate has also been previously tested in rodents by acute block of sympathetic and parasympathetic input to the heart. In spontaneously hypertensive rats, Oosting *et al*.[6] demonstrated that the circadian rhythm of heart rate is unaffected by pharmacological block of the autonomic nervous system. Makino *et al*.[7] reported that both sympathectomy and pharmacological block of the parasympathetic nervous system in rats diminishes but does not abolish the circadian variation in heart rate in rats. Knockout of the muscarinic M2 receptor or all three β-adrenergic receptors has little or no effect on the circadian rhythm in heart rate in mice.[8, 9] Taken together, these data call into question the widely accepted notion that autonomic tone is the *sole* driver of the circadian variation in heart rate. Here we tested the hypothesis that an intrinsic day-night rhythm in the sinus node (SN), the primary pacemaker of the heart, is an important contributor. We have focused on the pacemaker channel, HCN4, as a "first port of call".

METHODS

Animal models and associated ethical approval, experimental methods and statistical comparisons are described in detail in the Supplemental Methods.

RESULTS

Circadian variation in heart rate is independent of locomotor activity and persists under autonomic blockade

ECG telemetry in mice showed an *in vivo* day-night difference in mean heart rate and other electrophysiological variables including the PR interval and QRS duration – in Figure 1A the mean heart rate and other variables are plotted against the zeitgeber time (ZT), in which ZT 0 is taken as the start of the lights-on period. Changes in the heart rate set by the SN were explored: the heart rate was highest at ZT ~13 and it varied by 76±4 beats/min over the course of 24 h (Figure 1A; Supplemental Table 1). The day-night differences during the 12 h light:12 h dark lighting regime (shown by the alternating light and dark shading in Figure 1A) were sustained when the mice were placed in constant darkness (shown by the continuous dark shading in Figure 1A).

Mice are nocturnal and as expected lower physical (locomotor) activity was recorded from ZT 0 (lights-on) to ZT 12 (lights-off) compared to ZT 12 to ZT 0; this activity pattern continued in constant darkness (Figure 1A, bottom panel). Physical activity, if sufficiently intense and prolonged, is expected to influence the heart rate via the autonomic nervous system. Various methods were used to test whether the day-night difference in heart rate is an indirect result of the difference in physical activity (via the autonomic nervous system) or is an independent time-of-day effect. During 72 h of continuous recording in a normal light:dark cycle (Figure 1A), the heart rate and physical activity were averaged for each 5 min period for each animal. For ZT 0 – ZT 12 (day) and ZT 12- ZT 0 (night), the individual activity data were then binned into *No Activity* (0 arbitrary units, au) and *High Activity* (20-30 au) groups and the corresponding heart rate recorded. A mixed effects linear model showed that heart rate was significantly higher both at night (P=0.007) and when the mice were active (P<0.0001). However, the interaction between time and activity was not significant (P=0.27), which means that in this dataset the heart rate difference between night and day does not depend upon activity level. Comparisons were conducted between day and night at each of the activity levels using a 2-sided 5% test and applying a Sidak multiple comparison adjustment, and this revealed a significant difference (P=0.03) in the heart rate at night versus day in the *No Activity* group. Further details of these statistical tests are available in the Supplemental Results.

Exposing nocturnal animals to light during their active phase suppresses their locomotor activity, a phenomenon referred to as negative masking.[10, 11] Light pulses were used to separate the effects of time-of-day and physical activity. Figure 1B shows the heart rate and activity level in

conscious mice measured using telemetry before, during and after the light pulses (from Figure 1A, which shows the context of the selected data). In constant darkness, a 1 h light pulse from ZT 1 to ZT 2 was associated with a baseline level of physical activity and the heart rate was relatively low (Figure 1B). In contrast, a light pulse from ZT 13 to ZT 14 caused physical activity of the mice to fall to baseline values, whereas the heart rate remained relatively high (Figure 1B). Supplemental Figure 1 demonstrates no discernible relationship between heart rate and physical activity level before, during and after the light pulses or over 24 h. Therefore, in this experiment, the average heart rate of the nine mice was primarily influenced by the time-of-day rather than the average physical activity level. *In vivo*, the heart rate in the absence of physical activity was obtained by ECG recordings in anaesthetised mice at ZT 0 and ZT 12 - the heart rate was highest at ~ZT 12 and increased by 54±14 beats/min from ZT 0 (Figure 1C; Supplemental Table 1). It is concluded that in this study the effect of activity on the circadian rhythm in heart rate is not discernible.

Involvement of the autonomic nervous system in mediating the day-night variation in heart rate was tested by blocking cardiac muscarinic and β receptors (using 1 mg/kg atropine and 1 mg/kg propranolol; see Supplemental Discussion for justification of doses) in anaesthetised mice. The day-night difference in heart rate persisted after complete pharmacological autonomic block, although it was reduced in amplitude (Figure 1C; Supplemental Table 1). This *intrinsic* day-night difference in SN pacemaking was further confirmed in the isolated, denervated SN dissected at ZT 0 and ZT 12 (Figure 1D). The spontaneous SN beating rate remained higher at ZT 12 than ZT 0 – by 55±9 beats/min (Figure 1D; Supplemental Table 1). Next, the role of the vagus in setting the diurnal variation in heart rate *in vivo* was studied by two loss-of-function approaches: the SN is predominantly innervated by the right vagus[12] and its contribution to heart rate rhythmicity was assessed by unilateral right vagotomy in telemetrised rats. Figure 1E demonstrates that the day-night difference in heart rate persisted on sectioning the right vagus. The influence of vagal signalling (downstream of the muscarinic receptor) on the day-night rhythm was then investigated in *Girk4*$^{-/-}$ mice with genetic ablation of the acetylcholine-activated K^+ current ($I_{K,ACh}$). *Girk4*$^{-/-}$ mice exhibited slightly increased basal heart rates in comparison to wild-type counterparts, which is a typical hallmark of this genetic strain.[13] However, although $I_{K,ACh}$ is acknowledged to be a key mediator of the negative chronotropic effect of vagal stimulation on heart rate, loss of $I_{K,ACh}$ did not

perturb the circadian variation in heart rate in *Girk4*$^{-/-}$ mice *versus* control animals (Figure 1F; Supplemental Table 1).

Taken together, these findings demonstrate that the autonomic nervous system is not solely responsible for the day-night difference in heart rate *in vivo*. Intrinsic mechanisms underlying day-night rhythms were thus considered.

Day-night difference in HCN4 channel expression

Pacemaking is the result of the concerted action of ion channels and Ca^{2+}-handling proteins comprising the membrane and Ca^{2+} clocks and mRNA for many of these molecules (and key regulatory transcription factors) was measured in the SN by quantitative polymerase chain reaction (qPCR). Some transcripts, for example the pacemaker channel *Hcn4* (that carries the pacemaker current I_f), demonstrated a significant day-night difference (Figure 2A; Supplemental Table 2). With the exception of Ca^{2+}/calmodulin-dependent protein kinase IIδ (*Camk2d*), a day-night rhythm was not detected in any of the principal components of the Ca^{2+} clock (Figure 2A; Supplemental Table 2).

We focused on *Hcn4*, because of its central role in pacemaking in the SN.[14] *Hcn4* mRNA was measured at four time points. JTK Cycle, a statistical software tool for analysing circadian rhythms[15] shows that *Hcn4* mRNA displays a robust circadian rhythm and is at a maximum at ~ZT 20 (JTK Cycle, P=0.008; Figure 2B; Supplemental Table 3). To test whether this finding is associated with rhythmic *Hcn4* promoter activity, the 780 bp core promoter region of human *Hcn4*[16] was subcloned into a luciferase reporter construct (*h*Hcn4-Luc). Transient transfection of this construct into C2C12 cells was followed by forskolin treatment to synchronise circadian clocks across cultured cells.[17] As given in Figure 2C, real time bioluminescence recording (a measure of *Hcn4* promoter activation) revealed a discernible circadian rhythm of *h*Hcn4-Luc (JTK Cycle, $P=1.21 \times 10^{-14}$). Interestingly the phase of *h*Hcn4-Luc in synchronised cultured cells was comparable to HCN4 mRNA expression in the mouse SN (Figure 2B), peaking at circadian time (CT) ~19.5 (CT 0 is the time of forskolin treatment).

Expression of HCN4 protein in the SN at ZT 0, ZT 6 and ZT 12 was measured using western blot. A representative blot is shown in Figure 2D. HCN4 protein expression was normalised to total protein expression and is plotted versus time in Figure 3C – there was a

significant change at ZT 6 versus ZT 12. Supplemental Figure 2 shows examples of immunolabelling of HCN4 in tissue sections through the SN from wild-type mice culled at ZT 0 and ZT 12; the labelling was brighter, indicating higher expression, at ZT 12. This is confirmed by the mean data in Supplemental Figure 2. It is concluded that there is a circadian rhythm in HCN4 protein as well as the *Hcn4* transcript.

Role of HCN4 remodelling in the day-night difference in pacemaking

HCN4 is the primary channel underlying the funny current, I_f, and patch clamp experiments on isolated mouse sinus node cells were carried out to test whether there is a circadian rhythm in I_f. Figure 3A shows representative families of recordings of I_f from sinus node cells isolated from mice at ZT 0, ZT 6 and ZT 12. The density of I_f was reduced at ZT 6 compared to the earlier and later time points. Mean current density-voltage relationships from n=38, 31/38 and 24/27 cells (at ZT 0, ZT 6 and ZT12) are shown in Figure 3B – current density at ZT 6 was significantly reduced relative to that at ZT 12 at potentials $\leq$ -90 mV and ZT 0 at $\leq$ -105 mV. Current density at -120 mV is plotted against time in Figure 3D. Current density is calculated from current amplitude and cell capacitance and these measurements are plotted in Figure 3E,F. Cell capacitance did not vary with time, but current amplitude did, explaining the circadian rhythm in the density of I_f (Figure 3D-F).

To test whether rhythms in HCN4 and I_f contribute to the day-night difference in heart rate, HCN4 was blocked *in vivo* and in the isolated SN (efficacy and selectivity of blockers used is considered in the Supplemental Discussion). Telemetrised mice received an intraperitoneal injection of 6 mg/kg ivabradine to block HCN4 and thus I_f.[18] Block of I_f decreased the heart rate as expected (Figure 4A,B) and the effect of ivabradine on heart rate was greater at ZT 12 than ZT 0 (Figure 4A,B). Furthermore, as shown by the ECG recordings in Figure 4A and the summary data in Figure 4B, the presence of ivabradine abolished the day-night rhythm in heart rate *in vivo*. Analogous results were obtained *in vitro* by application of 2 mM Cs^+ to the isolated SN.[19] Once again, block of I_f by 2 mM Cs^+ decreased beating rate as expected, but the Cs^+ effect was greater at ZT 12 than ZT 0 (Figure 3C,D). In the presence of Cs^+, the day-night difference in beating rate was abolished (Figure 3D). These results suggest that HCN4 and I_f participate in the circadian rhythm in the intrinsic heart rate as well as heart rate *in vivo.*

A peripheral circadian clock in the SN

Circadian clocks are endogenous oscillators that generate transcriptional rhythms. In the ventricles there is an intrinsic circadian clock as well as a circadian rhythm in some ion channels.[1] qPCR showed that many canonical circadian clock genes are also present in the SN and their expression varies in the expected manner from ZT 0 to ZT 12 (Figure 5A). Two key circadian clock transcripts, *Bmal1* and *Clock*, were measured in the SN at four time points (BMAL1 and CLOCK form a heterodimer); Figure 5B shows that they demonstrated a robust daily rhythm and were at a maximum at ~ZT 0 (Supplemental Table 1). This suggests that a functional intrinsic circadian clock is contained in the SN. This was subsequently confirmed by measuring the bioluminescence in the isolated SN of *Per1*::LUC mice carrying a luciferase gene reporting the activity of *Per1*, a key circadian clock component (Figure 5C). *Per1*-driven bioluminescence fluctuated in the expected circadian manner and this periodicity was lost in $Cry1^{-/-}Cry2^{-/-}$ mice lacking a functional clock[20] (Figure 5C).

Role of the SN circadian clock in setting the day-night difference in *Hcn4* and intrinsic heart rate

To investigate a possible link between the local circadian clock in the SN and the circadian rhythm in the intrinsic heart rate, experiments were conducted on cardiomyocyte-specific *Bmal1* knockout mice. Knockout of *Bmal1* is known to disrupt the circadian clock[21] and previous studies have identified SN dysfunction on cardiomyocyte-specific *Bmal1* deletion.[e.g.22] Figure 6A confirms that, in these animals, *Bmal1* was effectively knocked out in the SN. Figure 6B shows that this disrupted the circadian rhythm in the expression of *Clock* mRNA – evidence that the SN circadian clock had been disrupted as expected (Supplemental Table 4). The intrinsic heart rate was measured in the isolated SN; *Bmal1* knockout mice presented with lower intrinsic heart rates *versus* wild-type mice and the normal day-night variation in intrinsic heart rate seen in wild-type mice was absent in *Bmal1* knockout mice (Figure 6C; wild-type data from Figure 1D). Furthermore, whereas there was a circadian difference in the reduction of the intrinsic heart rate on block of I_f by Cs^+ in wild-type mice (the effect of Cs^+ was greater at ZT 12 than ZT 0), in *Bmal1* knockout mice, once again, this pattern was lost (Figure 6D) – this suggests that there is a circadian variation in I_f, which is lost on disrupting the local circadian clock. Consistent with these observations, the ZT 0 to ZT 12 variation

in both *Hcn4* transcript and HCN4 protein (determined by immunolabelling) in wild-type mice was lost in the *Bmal1* knockout mice (Figure 6E,F and Supplemental Figure 2).

These findings suggest that the SN circadian clock controls intrinsic pacemaker activity via *Hcn4* transcriptional regulation. Mechanisms by which BMAL1 may regulate *Hcn4* were therefore investigated *in vitro.* The CLOCK::BMAL1 heterodimer acts as a transcriptional enhancer by binding to E-box binding sites in the promoter, intron or exon of a gene.[23] RVISTA was used to identify canonical E-box binding sites on *Hcn4.* Eight sites on *Hcn4* and 20 kb of its 5′ flanking region were identified (Figure 6G). *In vitro* ChIP was used to test whether BMAL1 specifically binds to these sites. ChIP enrichment for E-box binding sites D and G (within introns of the *Hcn4* gene; Figure 6G) were identified (Figure 6H). These data reveal potential direct interactions between the local SN clock and *Hcn4*.

DISCUSSION

For the first time, we show that the diurnal rhythm in heart rate in rodents cannot be fully attributed to oscillations in autonomic tone and reveal a day-night variation in intrinsic SN pacemaker activity. We define time-of-day variation in the expression of key pacemaking ion channels and ascribe particular physiological relevance to rhythmic *Hcn4* and associated I_f remodelling in setting the day-night variation in heart rate. Finally, we link, for the first time, SN pacemaking to an intrinsic circadian clock and propose a new role for BMAL1 as a transcriptional regulator of *Hcn*4.

This study has shown that there is a day-night difference in intrinsic SN pacemaker activity. Day-night differences in HCN4 mRNA and protein and I_f (Figures 2 and 3) accompanied the day-night variation in heart rate *in vivo* and intrinsic SN beating rate (Figure 1). Block of HCN4 and I_f by ivabradine *in vivo* and Cs^+ in the isolated SN was more pronounced at ZT 12 and HCN4 block abolished the day-night difference in heart rate *in vivo* and *ex vivo* (Figure 4). Data consistent with the time-of-day dependence of HCN4 block have been obtained from patients: in patients with inappropriate sinus tachycardia or ischaemic heart disease and heart failure, ivabradine causes a large decrease in heart rate during the day and little decrease at night.[24, 25] Nevertheless, I_f may not be the only mechanism involved: there was a day-night difference in Camk2d/CaMKIIδ expression and various K^+ channels, particularly Kcnh2/ERG/K_v11.1 (Figure 2A). Further study is warranted on the relative importance of these alterations in controlling SN pacemaking. Please

refer to the Supplemental Discussion for detailed limitations of the study.

This is the first report of a functioning circadian SN clock (Figure 5): key clock components were identified and many showed expected rhythms and phase relationships, e.g. *Bmal1* was downregulated, but *Cry2*, *Per1* and *Per2* were upregulated at ZT 12 *versus* ZT 0 (Figure 5A). This study provides the first evidence that *Hcn4* is under local clock control, as cardiac *Bmal1* knockout suppressed transcript abundance and abolished the day-night rhythm in both message and protein levels (Figure 6E,F). Functional BMAL1-binding E-box sites on *Hcn4* (Figure 6G,H) were identified and this is the first clue as to how the local clock exerts transcriptional control of pacemaking. Akin to the mouse, human *Hcn4* also includes one E-box consensus site within 5 kb of the 5′ flanking region and four sites within the first intron (Supplemental Figure 3). There is further discussion of the phasing of the circadian clock and *Hcn4*, HCN4 and I_f in the Supplemental Information.

CONCLUSION

In summary, this study has shown that a local clock driven day-night difference in intrinsic SN pacemaking contributes to the day-night difference in heart rate *in vivo*. Our findings provide new mechanistic insight into the fundamental question of why the heart rate of a mammal is lower when asleep and may explain the nocturnal occurrence of bradyarrhythmias in the human.

REFERENCES

1. Black N, D'Souza A, Wang Y et al. Circadian rhythm of cardiac electrophysiology, arrhythmogenesis, and the underlying mechanisms. Heart Rhythm 2019;16:298-307.

2. Sutherland GA. The pulse rate and range in health and disease during childhood. Quarterly Journal of Medicine 1929;22:519-529

3. Vandewalle G, Middleton B, Rajaratnam SM et al. Robust circadian rhythm in heart rate and its variability: influence of exogenous melatonin and photoperiod. Journal of Sleep Research 2007;16:148-155.

4. Monfredi O, Lyashkov AE, Johnsen AB et al. Biophysical characterisation of the under-appreciated and important relationship between heart rate variability and heart rate. Hypertension 2014;64:1334-1343.

5. Boyett M, Wang Y, D'Souza A. CrossTalk opposing view: Heart rate variability as a measure of cardiac autonomic responsiveness is fundamentally flawed. Journal of Physiology 2019;597:2599-2601.

6. Oosting J, Struijker-Boudier HA, Janssen BJ. Autonomic control of ultradian and circadian rhythms of blood pressure, heart rate, and baroreflex sensitivity in spontaneously hypertensive rats. Journal of Hypertension 1997;15:401-410.

7. Makino M, Hayashi H, Takezawa H, Hirai M, Saito H, Ebihara S. Circadian rhythms of cardiovascular functions are modulated by the baroreflex and the autonomic nervous system in the rat. Circulation 1997;96:1667-1674.

8. Swoap SJ, Li C, Wess J, Parsons AD, Williams TD, Overton JM. Vagal tone dominates autonomic control of mouse heart rate at thermoneutrality. American Journal of Physiology-Heart and Circulatory Physiology 2008;294:H1581-1588.

9. Kim SM, Huang Y, Qin Y, Mizel D, Schnermann J, Briggs JP. Persistence of circadian variation in arterial blood pressure in β1/β2-adrenergic receptor-deficient mice. American Journal of Physiology-Regulatory, Integrative and Comparative Physiology 2008;294:R1427-R1434.

10. LeGates TA, Altimus CM. Measuring circadian and acute light responses in mice using wheel running activity. Journal of Visualized Experiments 2011;48:e2463.

11. Fonken LK, Nelson RJ. The effects of light at night on circadian clocks and metabolism. Endocrine Reviews 2014;35:648-670.

12. Ng GA, Brack KE, Coote JH. Effects of direct sympathetic and vagus nerve stimulation on the physiology of the whole heart - a novel model of isolated Langendorff perfused rabbit heart with intact dual autonomic innervation. Experimental Physiology 2001;86:319-329.

13. Mesirca P, Marger L, Toyoda F, et al. The G-protein-gated K^+ channel, I_{KACh}, is required for regulation of pacemaker activity and recovery of resting heart rate after sympathetic stimulation. Journal of General Physiology 2013;142:113-126.

14. DiFrancesco D. The role of the funny current in pacemaker activity. Circulation Research 2010;106:434-446.

15. Hughes ME, Hogenesch JB, Kornacker K. JTK_CYCLE: an efficient nonparametric algorithm for detecting rhythmic components in genome-scale data sets. Journal of Biological Rhythms 2010;25:372-380.

16. Kuratomi S, Ohmori Y, Ito M et al. The cardiac pacemaker-specific channel Hcn4 is a direct transcriptional target of MEF2. Cardiovascular Research 2009;83:682-687.

17. Lowe M, Lage J, Paatela E, et al. Cry2 Is critical for circadian regulation of myogenic differentiation by Bclaf1-mediated mRNA stabilization of cyclin D1 and Tmem176b. Cell Reports 2018;22:2118-2132.

18. DiFrancesco D. Funny channels in the control of cardiac rhythm and mode of action of selective blockers. Pharmacological Research 2006;53:399-406.

19. Nikmaram MR, Boyett MR, Kodama I, Suzuki R, Honjo H. Variation in the effects of Cs^+, UL-FS 49 and ZD7288 within the sinoatrial node. American Journal of Physiology 1997;272:H2782-H2792.

20. van der Horst GT, Muijtjens M, Kobayashi K, et al. Mammalian Cry1 and Cry2 are essential for maintenance of circadian rhythms. Nature 1999;398:627-630.

21. Bunger MK, Wilsbacher LD, Moran SM et al. Mop3 is an essential component of the master circadian pacemaker in mammals. Cell 2000;103:1009-1017.

22. Schroder EA, Lefta M, Zhang X et al. The cardiomyocyte molecular clock, regulation of Scn5a, and arrhythmia susceptibility. American Journal of Physiology-Cell Physiology 2013;304:C954-965.

23. Ripperger JA, Schibler U. Rhythmic CLOCK-BMAL1 binding to multiple E-box motifs drives circadian Dbp transcription and chromatin transitions. Nature Genetics 2006;38:369-374.

24. Ptaszynski P, Kaczmarek K, Cygankiewicz I et al. The effect of ivabradine administration on the night drop of heart rate in patients with inappropriate sinus tachycardia. Journal of the American College of Cardiology 2018;71:392-392.

25. Grigoryan S, Hazarapetyan LG, Kocharyan SP. The influence of ivabradine on circadian pattern of heart rate and ischemic episodes in patients with ischemic heart disease and heart failure. European Heart Journal 2014;35:1012-1012.

FIGURE LEGENDS

Figure 1. The day-night difference in average heart rate is independent of average physical activity and autonomic tone. A, Heart rate, PR interval, QRS duration, uncorrected QJ interval and physical activity (measured using telemetry) in conscious mice (n=9) over ~6 days. Light and shaded regions represent light and dark phases in this and all similar figures. Timing of 1 h light pulses shown. In this and all similar figures, data are fit with a standard sine wave (red). Means±SEM shown in this and all other figures (except in case of physical activity - means±SD shown). **B,** *In vivo* heart rate and physical activity measured by telemetry at the times shown during 24 h darkness (subjective day and night is shown) with the exception of a 1 h light pulse delivered towards the start of the day (left) or night (right). The dotted red lines highlight the heart rate and physical activity at the end of the day-time light pulse and the red arrows highlight the heart rate at the end of the night-time light pulse. From the same experiment as A. **C**, *In vivo* heart rate measured from anaesthetised mice at ZT 0 and ZT 12 (n=9/9 mice) before (Control) and after autonomic block by intraperitoneal injection of 1 mg/kg atropine and 1 mg/kg propranolol. **D**, Spontaneous beating rate of the SN isolated at ZT 0 and ZT 12 (n=8/6 mice). **E,** *In vivo* heart rate at ZT 0 and ZT 12 measured by telemetry in vagotomised (n=7) rats at baseline (pre-surgery) and at 1, 3 and 7 days post-surgery. **F**, *In vivo* heart rate over 24 h measured in telemetrised wild-type control and *Girk4*$^{-/-}$ mice (n=21/23 mice). *P<0.05.

Figure 2. Day-night rhythms in SN ion channel profile and *Hcn4*. A, Relative expression of transcripts in the SN at ZT 12 (*versus* ZT 0; n=7/9 mice). The vertical line corresponds to 1, i.e. no change. Values <1 correspond to a decrease at ZT 12 and >1 an increase. **B**, Expression of *Hcn4* mRNA (normalised to expression of *Tbp* and *Ipo8*) in the SN at four time points over 24 h (n=6/6/6/6). **C,** Representative Lumicycle data (in arbitrary units) showing human *Hcn4* promoter activity over 24 h. **D**, Representative HCN4 western blot from the SN dissected at ZT 0, ZT 6 and ZT 12. A right atrial tissue sample (RA) is also shown as a negative control – as expected there is no HCN4 expression. Corresponding stain-free total protein gel used for quantification shown in lower panel.

Figure 3. Day-night rhythm in I_f. A, Families of recordings of I_f made from SN cells isolated at ZT 0, ZT 6 and ZT 12. **B**, Current-voltage relationships for I_f recorded from sinus node cells isolated at ZT 0 (n=38 cells/4 mice), ZT 6 (n=38 cells/3 mice) and ZT 12 (n=27 cells/5 mice). **C**, HCN4 protein expression from western blot ZT 0 (n=10), ZT 6 (n=5) and ZT 12 (n=10). Data pooled from two sets of independent experiments and protein expression is normalised to that at ZT 0. **D**, Density of I_f at -120 mV at ZT 0 (n=38 cells/4 mice), ZT 6 (n=38 cells/3 mice) and ZT 12 (n=27 cells/5 mice). **E**, Amplitude of I_f at -120 mV at ZT 0, ZT 6 and ZT 12 (same data as D). **F**, Cell capacitance at ZT 0, ZT 6 and ZT 12 (same data as D). *P<0.05.

Figure 4. Effect of HCN4 block on heart rate. A, Representative ECG recordings from telemetrised mice obtained at ZT 0 and ZT 12 at baseline and after the application of 6 mg/kg ivabradine. **B**, *In vivo* heart rate of wild-type mice measured at ZT 0 and ZT 12 before and after the administration of 6 mg/kg ivabradine (n=3/3). **C**, Representative extracellular potential recordings from the SN isolated at ZT 0 and ZT 12 at baseline and after the application of 2 mM Cs^+. **D**, Intrinsic heart rate of the isolated SN at ZT 0 and ZT 12 before and after the application of 2 mM Cs^+ (n=8/6/6/7). *P<0.05.

Figure 5. An intrinsic circadian clock in the SN. A, Relative expression of transcripts encoding key circadian clock components in the SN at ZT 12 *versus* ZT 0. The vertical line corresponds to 1, i.e. no change. Values <1 correspond to a decrease at ZT 12 and >1 an increase (n=7/9 mice). **B**, Expression of *Bmal1* and *Clock* mRNA in the SN at four time points over 24 h (n=6/6/7/8). **C**, Representative *Per1* activity (reported by luciferase bioluminescence) in the isolated SN from *Per1*::LUC mice on a $Cry1^{+/+}Cry2^{+/+}$ or $Cry1^{-/-}Cry2^{-/-}$ background. *P<0.05.

Figure 6. BMAL1 modulates intrinsic heart rate and HCN4. A and **B**, Expression of *Bmal1* (A) and *Clock* (B) at ZT 0 and ZT 12 in the SN of wild-type and *Bmal1* knockout mice (n= 6/7/5/6). **C**, SN beating rate at ZT 0 and ZT 12 from wild-type (n=8/6) and *Bmal1* knockout mice (n=3/3). **D**, Change in SN beating rate at ZT 0 and ZT 12 from wild-type (n=8/6) and *Bmal1* knockout mice on application of 2 mM Cs^+(n=3/3). **E** and **F**, Expression of *Hcn4* mRNA (E; n= 6/7/5/6) and HCN4

protein (F; determined by immunohistochemistry; arbitrary units; n=56/42/38/46 sections from 3/3/3/3 mice) in the SN of mice at ZT 0 and ZT 12. **G**, Diagram of *Hcn4* gene with 20 kb of the 5′ flanking region showing the position of eight potential E-box binding sites, A-H. **H**, Eight potential E-box binding sites pulled down on immunoprecipitation of His-tagged BMAL1 from Cos-1 cells transfected with His-tagged *Bmal1*. Data are normalised to immunoprecipitation from untransfected control cells; the red dashed line equals one and is the baseline level. *P<0.05 (binding site of interest versus binding site A; n=2 replicate experiments).

Figure 1

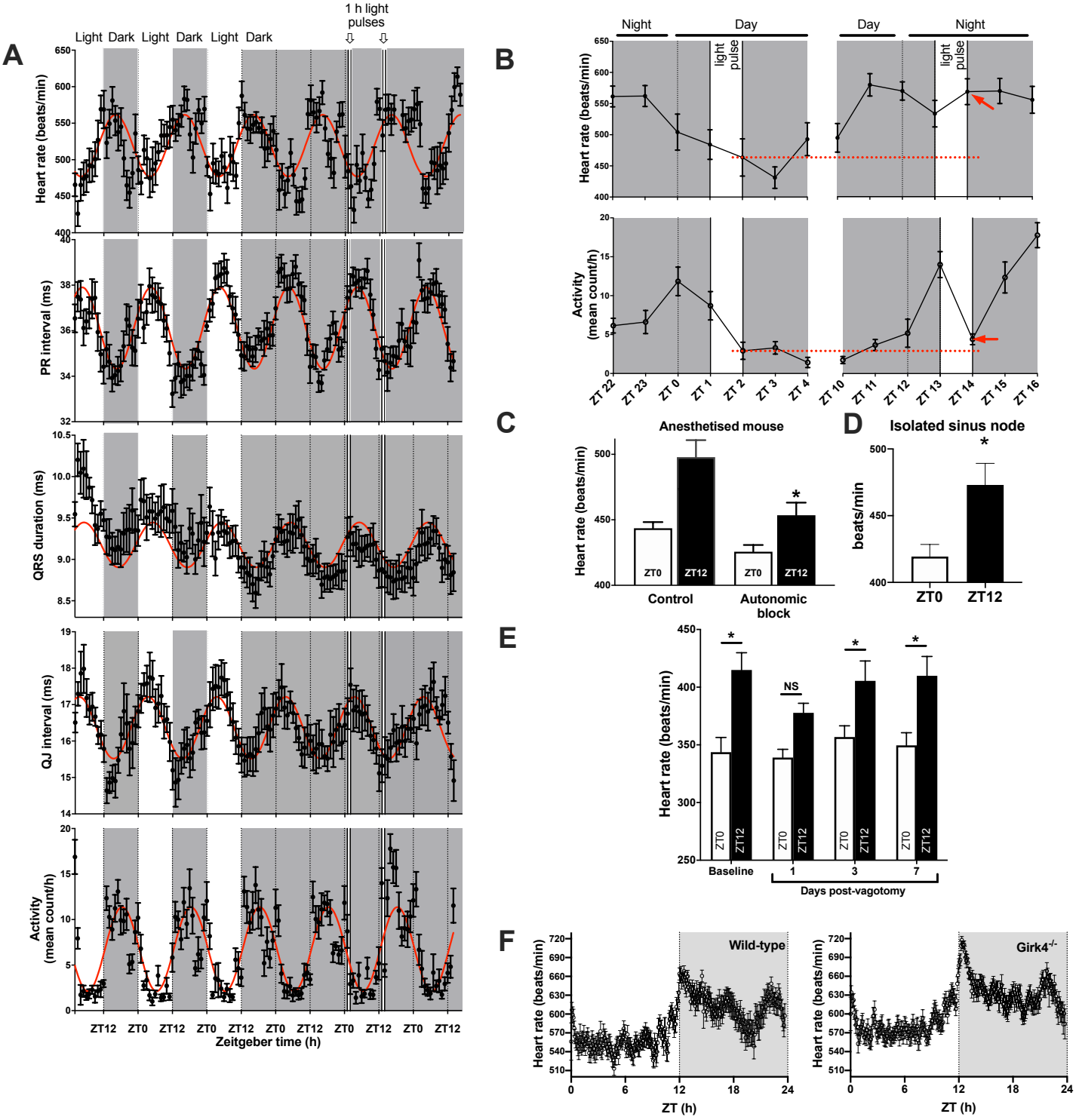
A
Light Dark Light Dark Light Dark
1 h light pulses
Heart rate (beats/min)
PR interval (ms)
QRS duration (ms)
QJ interval (ms)
Activity (mean count/h)
ZT12 ZT0 ZT12 ZT0 ZT12 ZT0 ZT12 ZT0 ZT12 ZT0 ZT12
Zeitgeber time (h)
B
Night Day Day Night
light pulse
Heart rate (beats/min)
Activity (mean count/h)
ZT 22 ZT 23 ZT 0 ZT 1 ZT 2 ZT 3 ZT 4 ZT 10 ZT 11 ZT 12 ZT 13 ZT 14 ZT 15 ZT 16
C
Anesthetised mouse
Heart rate (beats/min)
ZT0 ZT12 ZT0 ZT12
Control
Autonomic block
D
Isolated sinus node
beats/min
ZT0 ZT12
E
Heart rate (beats/min)
NS
Baseline
Days post-vagotomy
F
Wild-type
Girk4-/-
Heart rate (beats/min)
ZT (h)

Figure 2

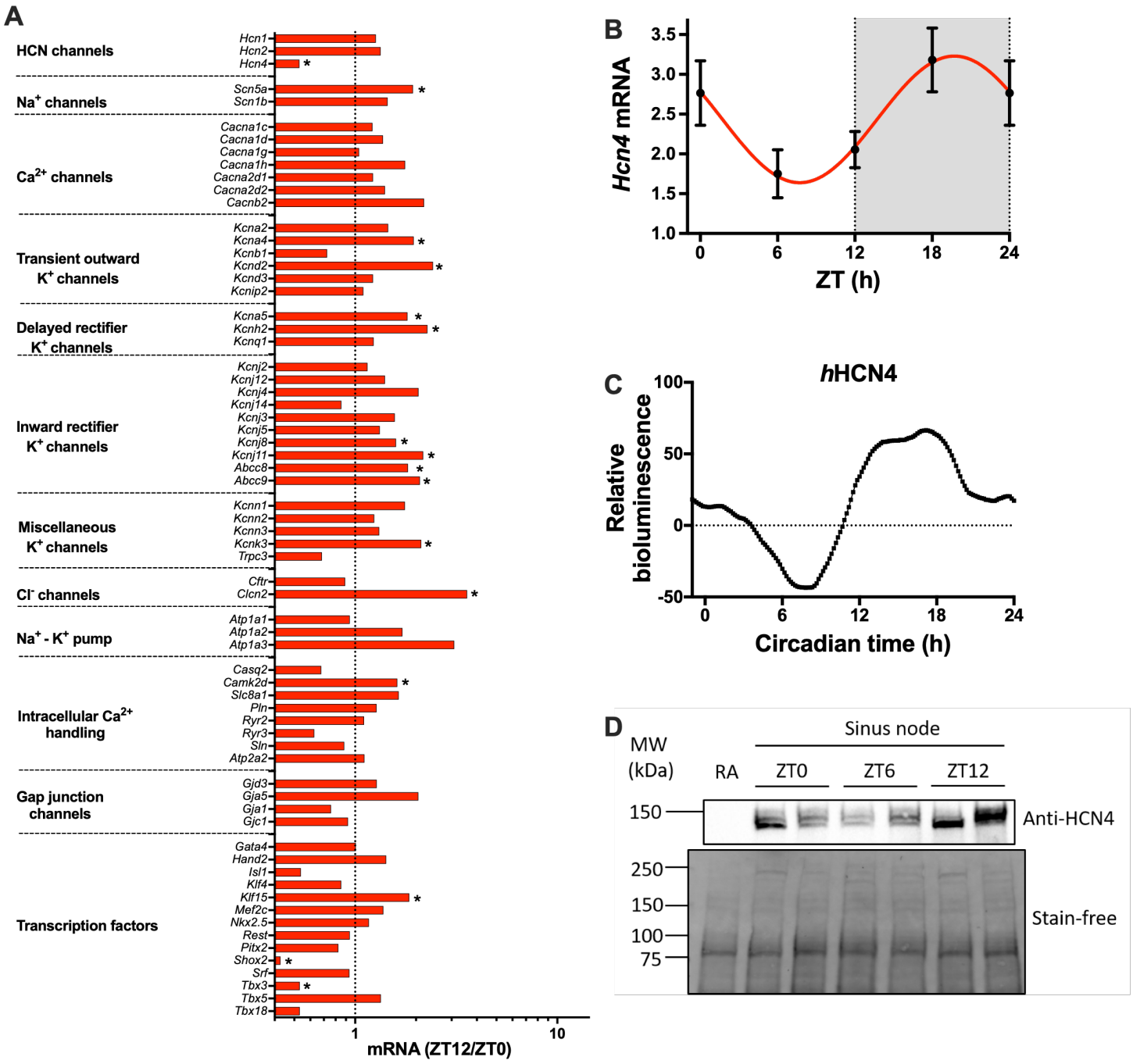
A
HCN channels
Hcn1
Hcn2
Hcn4
Na+ channels
Scn5a
Scn1b
Ca2+ channels
Cacna1c
Cacna1d
Cacna1g
Cacna1h
Cacna2d1
Cacna2d2
Cacnb2
Transient outward K+ channels
Kcna2
Kcna4
Kcnb1
Kcnd2
Kcnd3
Kcnip2
Delayed rectifier K+ channels
Kcna5
Kcnh2
Kcnq1
Inward rectifier K+ channels
Kcnj2
Kcnj12
Kcnj4
Kcnj14
Kcnj3
Kcnj5
Kcnj8
Kcnj11
Abcc8
Abcc9
Miscellaneous K+ channels
Kcnn1
Kcnn2
Kcnn3
Kcnk3
Trpc3
Cl- channels
Cftr
Clcn2
Na+ - K+ pump
Atp1a1
Atp1a2
Atp1a3
Intracellular Ca2+ handling
Casq2
Camk2d
Slc8a1
Pln
Ryr2
Ryr3
Sln
Atp2a2
Gap junction channels
Gjd3
Gja5
Gja1
Gjc1
Transcription factors
Gata4
Hand2
Isl1
Klf4
Klf15
Mef2c
Nkx2.5
Rest
Pitx2
Shox2
Srf
Tbx3
Tbx5
Tbx18
1
10
mRNA (ZT12/ZT0)
B
Hcn4 mRNA
3.5
3.0
2.5
2.0
1.5
1.0
0
6
12
18
24
ZT (h)
C
hHCN4
Relative bioluminescence
100
50
0
-50
0
6
12
18
24
Circadian time (h)
D
MW (kDa)
Sinus node
RA
ZT0
ZT6
ZT12
150
Anti-HCN4
250
150
100
75
Stain-free

Figure 3

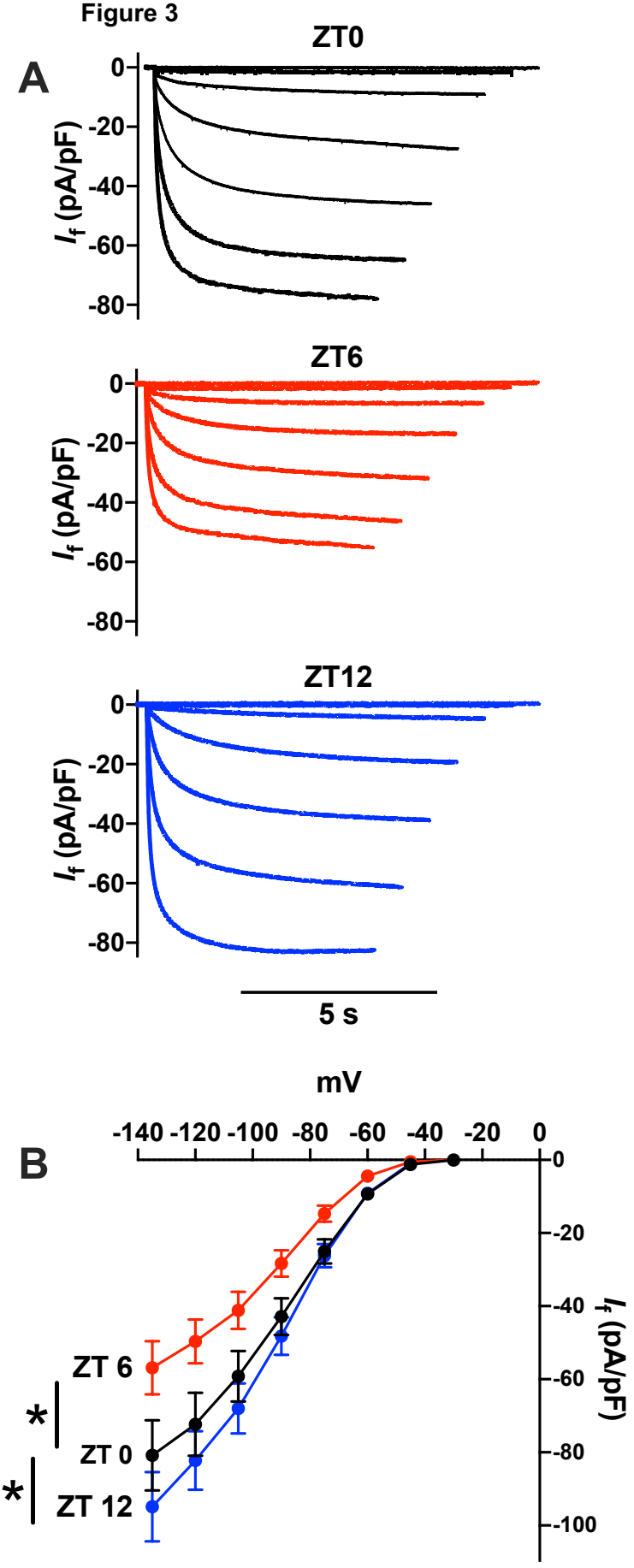
A
ZT0
ZT6
ZT12
I_f (pA/pF)
0
-20
-40
-60
-80
5 s
B
mV
-140 -120 -100 -80 -60 -40 -20 0
ZT 6
ZT 0
ZT 12
*
*
I_f (pA/pF)
C
HCN4 protein (au)
1.8
1.5
1.2
0.9
0.6
0.3
0.0
D
I_f (pA/pF)
80
60
40
20
0
E
I_f (pA)
2500
2000
1500
1000
500
F
C_m (pF)
40
30
20
10
0
0 3 6 9 12
ZT (h)

Figure 4

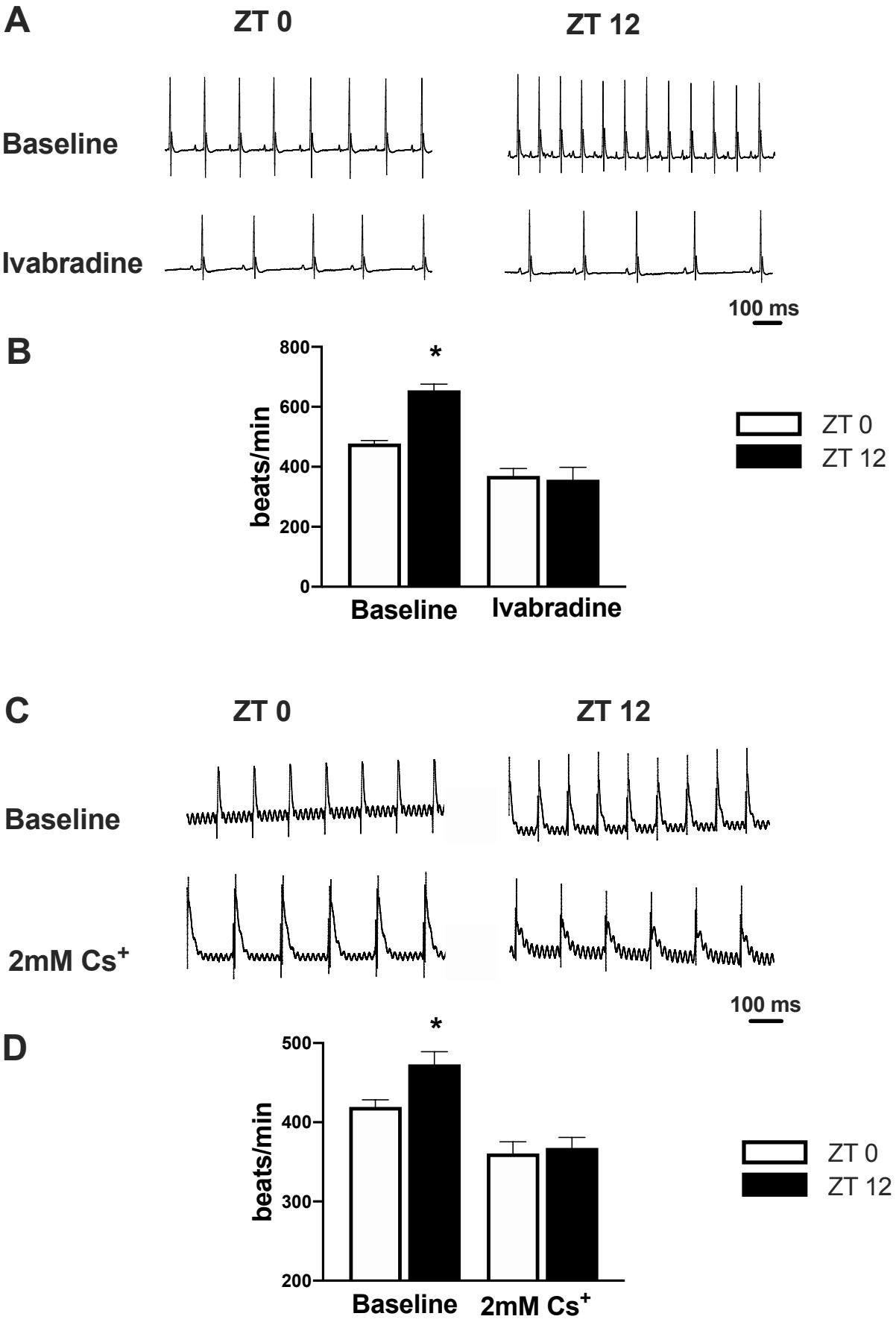
A
ZT 0
ZT 12
Baseline
Ivabradine
100 ms
B
800
600
400
200
0
beats/min
*
Baseline
Ivabradine
ZT 0
ZT 12
C
ZT 0
ZT 12
Baseline
2mM Cs+
100 ms
D
500
400
300
200
beats/min
*
Baseline
2mM Cs+
ZT 0
ZT 12

Figure 5

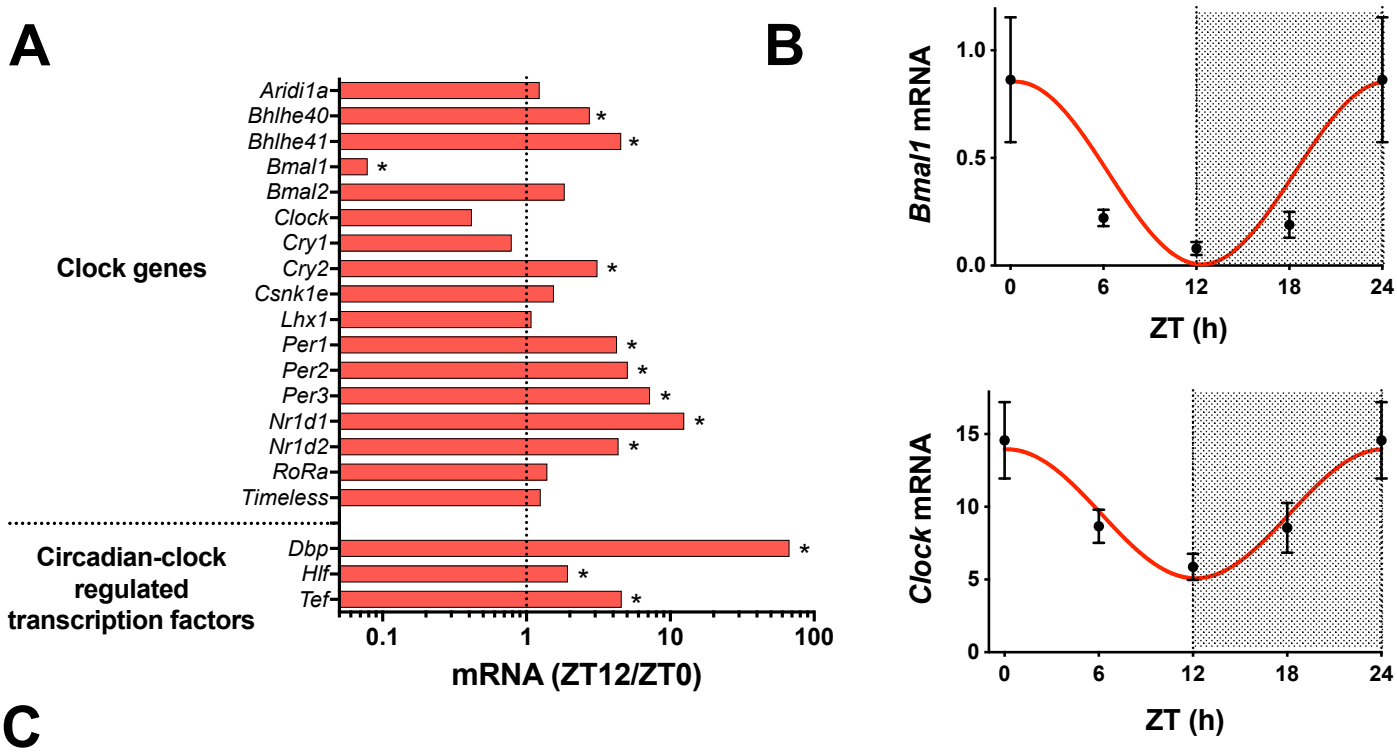
A
Clock genes
Aridi1a
Bhlhe40
Bhlhe41
Bmal1
Bmal2
Clock
Cry1
Cry2
Csnk1e
Lhx1
Per1
Per2
Per3
Nr1d1
Nr1d2
RoRa
Timeless
Circadian-clock regulated transcription factors
Dbp
Hlf
Tef
0.1
1
10
100
mRNA (ZT12/ZT0)
B
Bmal1 mRNA
1.0
0.5
0.0
0
6
12
18
24
ZT (h)
Clock mRNA
15
10
5
0
0
6
12
18
24
ZT (h)

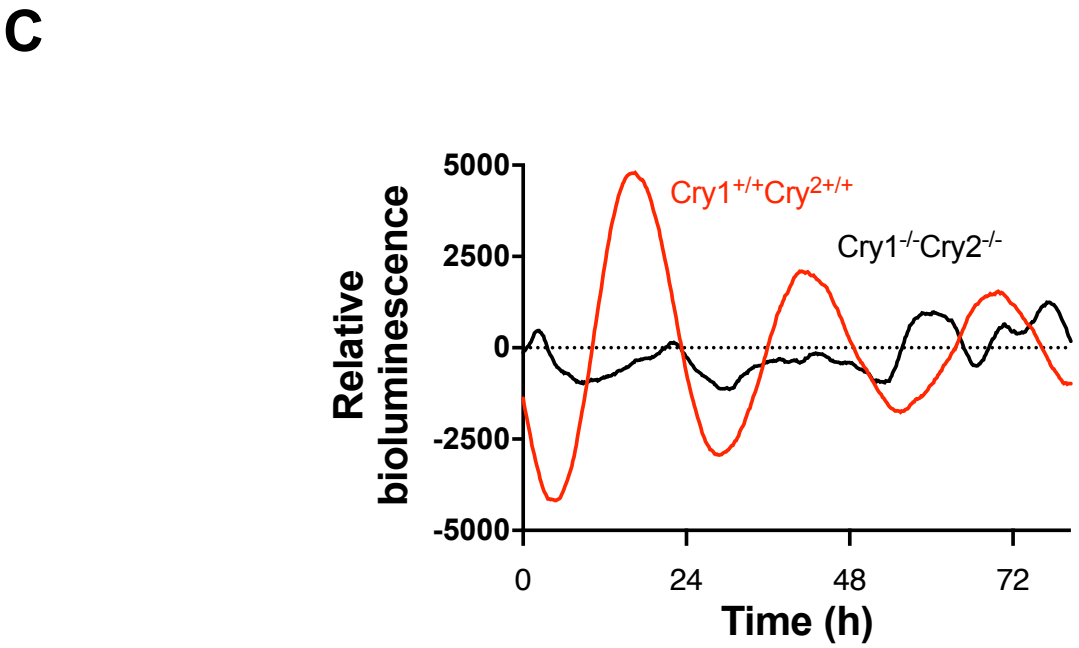
C
Relative bioluminescence
5000
2500
0
-2500
-5000
Cry1+/+Cry2+/+
Cry1-/-Cry2-/-
0
24
48
72
Time (h)

Figure 6

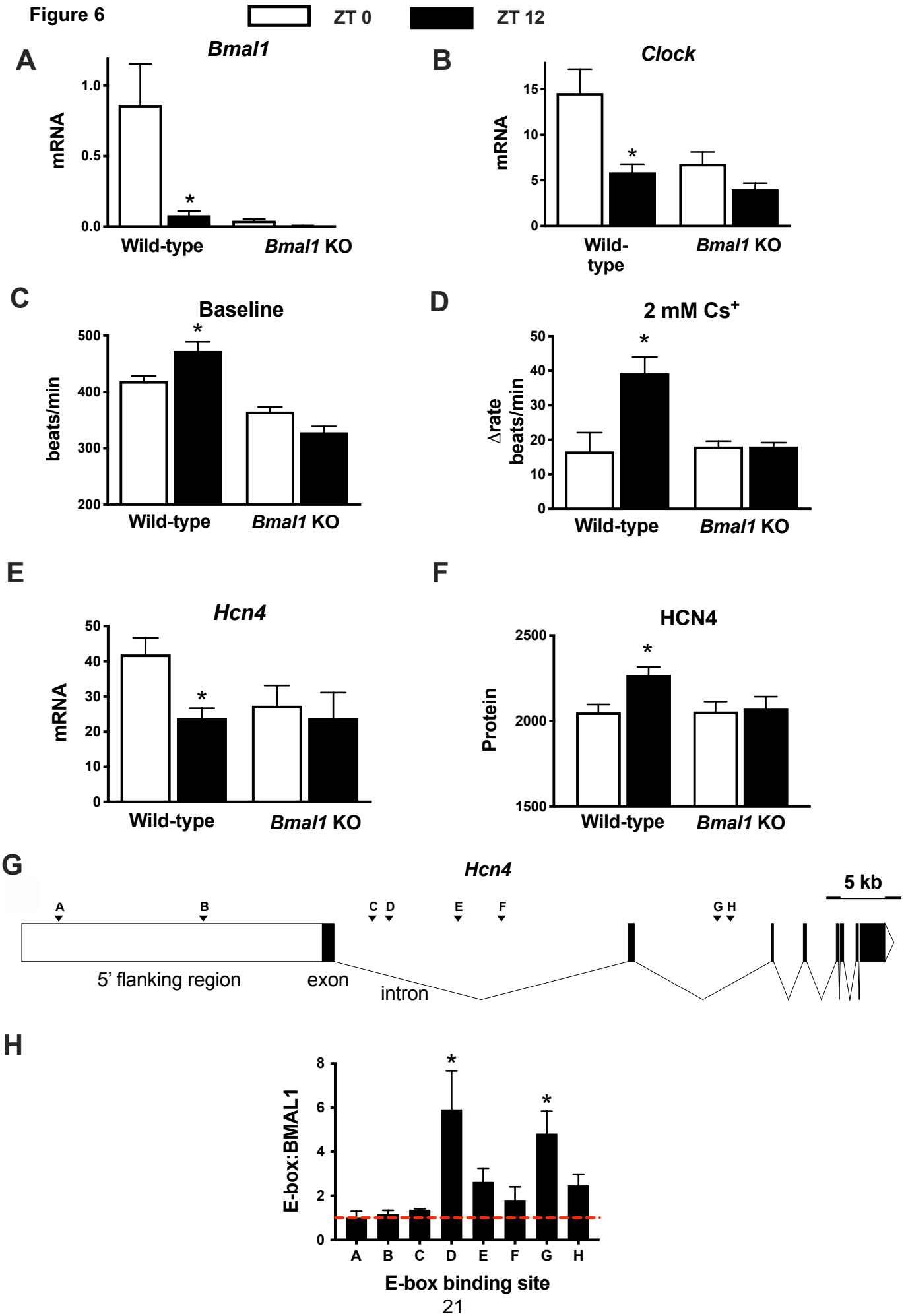
ZT 0
ZT 12
A
Bmal1
mRNA
1.0
0.5
0.0
*
Wild-type
Bmal1 KO
B
Clock
mRNA
15
10
5
0
*
Wild-type
Bmal1 KO
C
Baseline
beats/min
500
400
300
200
*
Wild-type
Bmal1 KO
D
2 mM Cs+
Δrate beats/min
50
40
30
20
10
0
*
Wild-type
Bmal1 KO
E
Hcn4
mRNA
50
40
30
20
10
0
*
Wild-type
Bmal1 KO
F
HCN4
Protein
2500
2000
1500
*
Wild-type
Bmal1 KO
G
Hcn4
5 kb
A
B
C D
E
F
G H
5' flanking region
exon
intron
H
E-box:BMAL1
8
6
4
2
0
*
*
A B C D E F G H
E-box binding site

SUPPLEMENTAL INFORMATION

Circadian clock in the sinus node mediates day-night rhythms in *Hcn4* and heart rate

Alicia D'Souza[1§]; Yanwen Wang[1]; Cali Anderson[1]; Annalisa Bucchi[2]; Mirko Barsucotti[2]; Servé Olieslagers[3]; Pietro Mesirca[4,5]; Anne Berit Johnsen[6]; Svetlana Mastitskaya[7]; Haibo Ni[8]; Yu Zhang[1]; Nicholas Black[1]; Charlotte Cox[1]; Sven Wegner[1]; Beatriz Bano-Otalora[1]; Cheryl Petit[1]; Eleanor Gill[1]; Sunil Jit Logantha[1,9]; Halina Dobrzynski[1,10]; Nick Ashton[1]; George Hart[1]; Rai Zhang[11] Henggui Zhang[8]; Elizabeth J Cartwright[1]; Ulrik Wisloff[6]; Matteo E. Mangoni[4,5]; Paula Da Costa Martins[3]; Hugh D. Piggins[12]; Dario DiFrancesco[2,13]; Mark R. Boyett[14]

[1]Division of Cardiovascular Sciences, University of Manchester, UK. [2]Department of Biosciences, University of Milan, Italy. [3]Faculty of Health, Medicine and Life Science, Maastricht University, Netherlands. [4]Institut de Génomique Fonctionnelle, Université de Montpellier, CNRS, INSERM, Montpellier, France. [5]LabEx Ion Channels Science and Therapeutics (ICST), France. [6]Department of Circulation and Medical Imaging, Norwegian University of Science and Technology, Norway. [7]Neuroscience, Physiology and Pharmacology, University College London, UK. [8]School of Physics and Astronomy, University of Manchester, UK. [9]Liverpool Centre for Cardiovascular Science and Department of Cardiovascular and Metabolic Medicine, University of Liverpool, UK. [10]Department of Anatomy, Jagiellonian University Medical College, Poland. [11]School of Civil, Aerospace and Mechanical Engineering, University of Bristol, UK. [12]School of Physiology, Pharmacology & Neuroscience, University of Bristol, UK. [13]IBF-CNR, Italy. [14]Department of Biomedical Sciences, Faculty of Health and Medical Sciences, University of Copenhagen, Denmark

Abbreviations

Hcn4: hyperpolarisation-activated cyclic nucleotide-gated channel 4 gene and transcript
HCN4: hyperpolarisation-activated cyclic nucleotide-gated channel 4 protein
HRV: heart rate variability
I_f: funny current
$I_{K,ACh}$: acetylcholine (ACh)-activated K^+ current
qPCR: quantitative polymerase chain reaction
SN: sinus node
ZT: zeitgeber time
Initial capital and then lower-case letters in italics: gene and transcript
Capital letters: protein

SUPPLEMENTAL METHODS

Ethical approval

In Norway, the telemetry study was approved by the Norwegian Council for Animal Research, in accordance with the Guide for the Care and Use of Laboratory Animals from the European Commission Directive 86/609/EEC. Ethical approval for vagotomy in rats was granted by University College London and the experimental procedures were in accordance with the UK Animals (Scientific Procedures) Act 1986. Ethical approval for telemetry in Girk4$^{-/-}$ mice was approved by the Ethical committee of the University of Montpellier and the French Ministry of Agriculture (protocol n°: 2017010310594939). All remaining procedures were approved by the University of Manchester, in accordance with the UK Animals (Scientific Procedures) Act 1986. Mice were sacrificed by cervical dislocation and rats were sacrificed by overdose with pentobarbital.

Experimental animals

Mice were housed five per cage in a temperature-controlled room (22°C) with a 12 h:12 h light:dark lighting regime (unless stated otherwise) and free access to food and water. Lights-on was at zeitgeber time (ZT) 0 and lights-off at ZT 12. Mice were adapted to a lighting regime for at least two weeks before use. Mice were sacrificed by cervical dislocation at defined time points, e.g. ZT 0; during the dark period, mice were handled with the aid of night vision goggles to prevent exposure of the mice to light. The majority of experiments were carried out using male 10-12 week old (initial age) 25-30 g C57BL/6J mice from Harlan Laboratories. *Cry*$^{+/-}$*Cry2*$^{+/-}$mice[1] that had been bred with transgenic knock-in animals (*Per1*::LUC), in which luciferase expression is driven by the mouse *Per1* promoter and 5'-UTR elements,[2] were originally obtained from Professor G.T. van der

Horst (Erasmus MC, Rotterdam, Netherlands). Adult male offspring mice lacking the core molecular circadian clock (deficient in the *Cryptochrome* genes *Cry1*$^{-/-}$*Cry2*$^{-/-}$) and their congenic male wild-type littermates (*Cry1*$^{+/+}$*Cry2*$^{+/+}$) in which the molecular clock is fully functional were used at 4-6 months of age as described previously.[3] 21 wild-type (C57B/6J from Charles River) and 23 Girk4$^{-/-}$ mice,[4] 23±1 weeks of age with matched sex ratio (50%), were bred in a specific pathogen free (SPF) animal facility of the Institut de Génomique Fonctionnelle, Montpellier, France on a C57B/6J genetic background. Male 10-14 week old cardiac-specific *Bmal1* knockout mice were used. They were generated by breeding *Bmal1*$^{flox/flox}$ mice with α-myosin heavy chain-Cre mice. *Bmal1*$^{flox/flox}$ mice have loxP sites flanking exon 8 of the *Bmal1* gene (Jackson Labs 007668)[5] and the cardiomyocyte-specific α-myosin-heavy chain (*Myh6*) promoter drives expression of Cre recombinase in the α-myosin heavy chain Cre mice.[6] In the resulting offspring, the exon encoding the *Bmal1* basic helix-loop-helix (bHLH) domain was deleted in the Cre recombinase-expressing cardiac tissues. Details of rats used are given below.

ECG and activity recording via telemetry in mice

For the experiment shown in Figure 1A, mice were anaesthetised with isoflurane (2.5% in O_2) and sterilised remote radio telemetry transmitters (model TA11ETA-F10, Data Sciences International, Netherlands) were implanted into the peritoneal cavity. Two electrodes were subcutaneously placed on the left caudal rib region and right pectoral muscle. Following surgery, mice were single-housed at 37°C for 2 h and then transferred to the normal holding area for one week to allow recovery. The ECG and activity were continuously recorded for six days. Activity (in arbitrary units, au; usually 0–30 au) was calculated by the recording system based on alterations in transmitter signal strength, which changes with locomotor activity. Animals were maintained in a normal 12 h:12 h light:dark cycle for the first three days and in constant darkness for the remainder of the experiment, during which 1 h light pulses were given at ZT 1-2 and ZT 13-14 on Day 5. Telemetry data were received by small animal receiver RPC-1 (Data Sciences International), amplified by a Data Exchange Matrix (Data Sciences International) and acquired by Data Quest A.R.T. (P3 Plus version 4.8, Data Sciences International). For Figure 1A, the ECG and physical activity were recorded for 12 min every hour. The ECG was analysed using LabChart 7 (ADInstruments). First, we averaged 100 beats. Typical ECG variables were then automatically measured (with discretion for manual refinement) using LabChart. The RR interval was measured as the interval between the peaks of consecutive R waves. The PR interval was measured as the interval between the start of the P wave and the start of the Q wave. The duration of the QRS complex was measured as the interval between the start of the Q wave and the point at which the S wave returned to the zero-voltage axis. The start point of the QT interval was taken as the beginning of the Q wave. The end point of the QT interval was taken as the time at which the last discernible wave crossed the zero-voltage axis. In the mouse, the QRS complex is followed by a positive T wave (or 'J' wave) and this can be followed by a negative T wave. A recent study showed that, in the mouse, ventricular action potential duration at 90% repolarization coincides well with the end of the positive T wave or J wave when the negative T wave is absent.[7] For further discussion see Boukens *et al.*[8] In this study, the QT (or QJ) interval was measured in this way, because a negative T wave was generally not discernible. ECG data shown in Figure 1A are smoothed (2 h moving average). For statistical analysis of the relationship between heart rate and activity, mean heart rate and activity were recorded every 5 min over the six days.

The heart rates of mice shown in Figure 1F were obtained in a separate experiment. The details of the telemetry are given by Mesirca *et al*.[9]

The effect of ivabradine shown in Figure 4A,B was investigated in a third experiment. Telemetry transmitters (PhysioTel^{TM} ETA-F10, DSI) were implanted subcutaneously under isoflurane inhalation anaesthetic (induced at 2% and maintained at 1.5% in 100% O_2) in C57BL/6J mice (aged 8-10 weeks at time of surgery). Animals were allowed to recover from surgery for 5 days after which ECG signals were recorded at 2 kHz continuously over six days using Ponemah software (DSI). The baseline recording took place over 53 h (i.e. >2 circadian cycles). The effect of ivabradine on day-night heart rate was studied by administration of a 6 mg/kg I.P. injection at ZT 0 and ZT 12. The average heart rate for 30 min, starting 10 min after injection was compared to a time-matched 30 min recording from a baseline cycle.

Telemetry and vagotomy in rats

Biotelemetry was used to record systemic arterial blood pressure and heart rate in vagotomised male 300-350 g Sprague-Dawley rats. Animals were anaesthetised with isoflurane (3% in O_2) and a laparotomy was performed to expose the abdominal aorta. A catheter connected to a telemetry pressure transducer (model TA11PAC40, DSI) was advanced rostrally into the aorta and secured with Vetbond (3M). The transmitter was secured to the abdominal wall and the incision was closed by successive suturing of the abdominal muscle and skin layers. Carprofen was given and the animals were returned to their home cages where they were allowed to recover for at least seven days. After the recovery period of one week and following recordings of the baseline haemodynamic parameters for 24 h, the animals were anaesthetised with isoflurane (3% in O_2). Using an aseptic technique, an anterior midline neck incision was performed, the sternohyoid and sternocleidomastoid muscles were retracted and the right cervical vagus nerve was isolated and sectioned. Sham-operated rats underwent the same surgical procedures to expose the nerve, but the vagus was left intact. Heart rate was recorded for seven days after surgery.

ECG recording from the anaesthetised mouse

Mice were anaesthetised with isoflurane (2% in O_2). A three-lead ECG was recorded using LabChart 7. Positive and negative electrodes were placed subcutaneously on the right fore limb and hind limb, respectively, and a reference electrode was placed subcutaneously on the left hind limb. ECG parameters were measured using LabChart 7 and GraphPad Prism. After 10 min (to allow the heart rate to stabilise), the ECG was recorded for 2 min and the average heart rate calculated. Block of the autonomic nervous system was achieved by intraperitoneal injection of propranolol (1 mg /kg), followed by intraperitoneal injection of atropine (1 mg /kg) after ~15 min or when the effect of sympathetic block with propranolol had reached steady-state. After a further ~5 min (once a steady-state, post atropine administration, had been reached), the ECG was recorded for a 5 min and the average heart rate calculated.

Electrogram recording from the isolated sinus node

Following sacrifice, the heart was removed and the rear wall of the right atrium encompassing the sinus node was rapidly dissected. The preparation was superfused with Tyrode's solution (containing in mM: 100 NaCl, 4 KCl, 1.2 $MgSO_4$, 1.2 KH_2PO_4, 25 $NaHCO_3$, 1.8 $CaCl_2$; 10 glucose; equilibrated with 95% O_2 and 5% CO_2 to give a pH of 7.4) at 37°C at a flow rate of 10 ml /min. An electrogram was recorded using three electrodes: two electrodes pinned either side of the preparation and a third earth electrode. Recordings were amplified using a Neurolog system with low-pass and high-pass filters adjusted to optimise the signal-to-noise ratio. Electrograms were recorded and analysed using LabChart 7 and GraphPad Prism. After dissection, the preparation was allowed to stabilise for 15 min, after which the electrogram was recorded and the average beating rate calculated over 10 min. The superfusing solution was changed to Tyrode's solution containing 2 mM CsCl. After 15 min of treatment, the electrogram was again recorded and the average beating rate calculated.

Isolation of sinus node cells and I_f recording and analysis

All procedures conformed to Italian and European laws (D. Lgs n° 2014/26, 2010/63/UE) and were approved by the University of Milan Animal Welfare Body and by the Italian Minister of Health. Cells used in these experiments were obtained from C57BL/6J male mice kept in 12 h:12 h light:dark conditions. On the day of an experiment, mice were euthanised by cervical dislocation and the heart quickly extracted and placed in Tyrode's solution (mM: NaCl, 140; KCl, 5.4; $CaCl_2$, 1.8; $MgCl_2$, 1; D-glucose, 5.5; HEPES-NaOH, 5; pH 7.4) with heparin (10 U/ml). This procedure was carried out at ZT 0, ZT 6, and ZT 12 corresponding to 7 am, 1 pm and 7 pm, respectively. After the dissection of the sinus node region, cells were isolated following an enzymatic and mechanical dissociation procedure as previously described.[10] Isolated single cells were kept at 4°C in Tyrode's solution for the day of the experiment and patch-clamp experiments were performed in the whole-cell configuration at 35±0.5°C. I_f was recorded from single cells superfused with Tyrode's solution containing $BaCl_2$ (1 mM) and $MnCl_2$ (2 mM). The pipette solution contained (in mM): K-aspartate, 130; NaCl, 10; EGTA-KOH, 5; $CaCl_2$, 2; $MgCl_2$, 2; ATP (Na^+-salt), 2; creatine phosphate, 5; GTP (Na^+-salt), 0.1; pH 7.2. Current densities were calculated by normalising the steady-state amplitudes recorded during a train of seven hyperpolarizing steps (range: from – 30

mV/10 s to 120 mV/5.8 s; increment between steps, -15 mV and -700 ms; holding potential, -30 mV) to cell capacitance.

RNA isolation and quantitative polymerase chain reaction (qPCR)

A ~1 mm biopsy was collected from the sinus node at the level of the main branch of the crista terminalis, rapidly frozen in liquid N_2 and stored at −80°C until use. Total RNA was isolated using an RNeasy Micro kit (Qiagen). RNA purity and quantity were determined using a NanoDrop ND-1000 spectrophotometer (NanoDrop Technologies). Synthesis of cDNA was performed using the Superscript VILO cDNA Synthesis Kit (ThermoFisher Scientific) using the manufacturer's protocol in which 150 ng of RNA in 14 μl of dH_2O was added to 4 μl 5x VILO Reaction mix + 2 μl 10x RT SuperScript Enzyme mix. qPCR was carried out using an ABI Prism 7900 HT Sequence Detection System (Applied Biosystems/Life Technologies Corporation). The expression level of 88 transcripts was measured using custom-designed Taqman Low Density Array Cards (Applied Biosystems, catalogue number 4342259; format 96A) as previously described[11] and according to the manufacturer's instructions. Briefly, 150 ng of cDNA and TaqMan Universal Master Mix (Applied Biosystems) were loaded into each port of microfluidic cards containing fluorogenic TaqMan probes and primers. Thermal cycling conditions were 50°C for 2 min and 94.5°C for 10 min, followed by 40 cycles at 97°C for 30 s and 59.7°C for 1 min. Data were collected with ABI Prism 7900 HT Sequence Detection System software (SDS 2.3) and analysed using RealTime Statminer (v4.1, Integromics). Expression levels of the housekeeping genes, *18s*, *Gapdh*, *Hmbs*, *Ipo8*, *Pgk1* and *Tbp*, were tested. *Ipo8* and *Tbp* were selected as optimal (most stable) endogenous controls using geNorm, NormFinder and Minimum Variance Median via RealTime Statminer. Transcript expression levels were calculated using the ΔCt method. Statistical significance was tested using the non-parametric limma test and Benjamini–Hochberg False discovery rate correction set at 5%. For single assays, the qPCR reaction mixture comprised 1 µl cDNA, 1× Qiagen assay (*Bmal1*, QT00101647; *Clock*, QT00197547; *Hcn4*, QT00268660; *Ipo8*, QT00291977; *Tbp*, QT00198443), 1× SYBR Green Master Mix (Applied Biosystems) and DNase-free water. All samples were run in duplicate. Mean delta Ct values ($Ct_{reference\ gene}/Ct_{gene\ of\ interest}$) for *Hcn4*, *Bmal1* and *Clock* and corrrsponding Ct values for the reference transcripts, *Ipo8* and *Tbp1*, in individual runs of single-assay qPCR data are given in Supplemental Tables 3 and 4. Data in all graphs are normalised to expression of reference genes *Ipo8 and Tbp.* The reaction conditions were: denaturation step of 95°C for 10 min followed by 40 cycles of amplification and quantification steps of 95°C for 30 s, 60°C for 30 s and 72°C for 1 min. The melt curve conditions were: 95°C for 15 s, 60°C for 15 s and 95°C for 15 s. mRNA expression normalised to the expression of the housekeepers, *Ipo8* and *Tbp*, was calculated using the ΔCt method.

Bioluminescence experiments

(i) ***h*HCN4-Luc.** The previously characterised human *Hcn4* promoter region spanning from bp −267 to +157 (the number is the distance in base pairs from the putative transcription start site, +1)[12] was amplified by PCR, and the product was ligated into the pGL3-Basic luciferase reporter vector (Promega). C2C12 cells were maintained in Dulbecco's Modified Eagle's Medium (DMEM) supplemented with 10% (v/v) foetal bovine serum (FBS) and 1% (v/v) penicillin-streptomycin and passaged using 0.25% trypsin-EDTA. 2×10^5 cells were seeded in transparent 35 mm Petri dishes and grown to 70% confluence prior to transfection with 1 μg pGL3-*h*HCN4 (luciferase reporter for the 780 bp 5′ flanking region of human HCN4), using 6 μl Lipofectamine 2000. As a positive control, cells were transfected with *mPer2:Luc* or *mBmal1:Luc* with the addition of transposase (0.5 µg) to catalyse the transposition mechanism of these constructs (data not shown). At 5 h post-transfection, the medium was replaced with serum-free DMEM and cells cultured overnight. Forskolin (1 h, 10 µM) was used to synchronise the molecular clocks of the cells.[13] Subsequently, cells were washed twice in phosphate buffered saline (PBS) before the addition of recording medium: serum-free DMEM without phenol red (Sigma), 4.2 mM $NaHCO_3$ (Sigma), 10 mM HEPES (Sigma), 1% v/v penicillin-streptomycin (Sigma), 2% v/v B27 (Gibco) and 0.1 mM luciferin. Petri dishes were sealed using high vacuum grease (Dow Corning) and 40 mm round glass cover slips. Bioluminescence was recorded every 10 min for 96 h in a Lumicycle luminometer (Actimetrics) placed inside an incubator at 37°C. Photon counts were integrated for 599 s every 600 s. Bioluminescence data were detrended by subtracting a 24 h running average from the raw data and smoothed with a 3 h running average. The non-parametric JTK_Cycle algorithm[14] was used to statistically determine the presence of circadian rhythmicity within a 24 h period.

***(ii) Per1*::LUC.** Total bioluminescence was recorded for 96 h from individual intact sinus

node preparations using photomultiplier tube assemblies (H8259/R7518P, Hamamatsu) using previously described methods.[15] 3.5 cm dishes were prepared under sterile conditions with a layer of autoclaved high-vacuum grease (Dow Corning) on the top rim, a Millicell insert (Millipore) and 1 ml recording medium consisting of DMEM (Invitrogen) supplemented with 10% foetal calf serum (FCS) and 1% penicillin/streptomycin and 0.1 mM luciferin in autoclaved Milli-Q water. A freshly dissected beating sinus node was placed on the Millicell insert following which the dish was sealed with a glass coverslip and placed into the photomultiplier tube assembly housed in a light-tight incubator (GalaxyR+; RS Biotech) and maintained at 37°C. Photon counts were integrated for 599 s every 600 s. Bioluminescence data were detrended by subtracting a 24 h running average from the raw data and smoothed with a 3 h running average.

Western blot

Snap frozen sinus node biopsies were homogenised using MP FastPrep-24 and 2 ml tubes containing FastPrep metal bead lysing matrix (1.4 mm) in RIPA buffer (Sigma Aldrich). Western blotting for HCN4 protein was conducted in two separate experiments. In the first set, Bradford protein assay was used to estimate total protein concentration following which samples were denatured using 25% SDS-sample buffer (100 mM Tris-HCl, pH 6.8, 25% v/v glycerol, 10% v/v SDS, 10% v/v β-mercaptoethanol, 0.1% w/v bromophenol blue) and heating to 80°C for 10 min. Proteins were separated using a 7.5% stain-free SDS-polyacrylamide gel electrophoresis (PAGE) (Bio-Rad) system with Precision Plus (Bio-Rad) protein standards running at 50 mV for ~50 min in SDS running buffer (25 mM Tris, 192 mM glycine, 0.1% SDS). In the second set of experiments Pierce BCA protein assay was used to estimate total protein concentration in homogenised sinus node biopsies following which samples were denatured in 2x Laemmli buffer (Sigma) containing 6 M urea and heating to 37°C for 15 min. Proteins were separated using a 4-20% stain-free SDS-polyacrylamide gel electrophoresis (PAGE) system (Bio-Rad) with Precision Plus Unstained Protein Standards (*Strep*-tagged recombinant, Bio-Rad) running at 110 V for ~70 min in SDS running buffer. Gels were imaged using ChemiDoc MP and proteins transferred to PVDF (polyvinyl difluoride) membranes using the Trans-Blot Turbo transfer system (Bio-Rad) at 15 V/0.3 mA for 15 min according to the manufacturer's instructions. Successful transfer was confirmed by imaging using the ChemiDoc MP. PVDF membranes were washed in Tris-buffered saline (TBS) and blocked in milk-TBS-Tween (5% w/v non-fat dried Marvel milk, TBS, 0.1% v/v Tween 20) and probed with the following primary antibodies for 1 h at room temperature with gentle rocking: rabbit polyclonal anti-HCN4 (Alomone Labs), 1:100; rabbit polyclonal anti-actin (Sigma Aldrich), 1:1000. After washing, membranes were then probed with horseradish peroxidase (HRP)-linked secondary antibody (HRP-linked anti-rabbit IgG, Cell Signalling). Unbound secondary antibody was removed by washing in TBS-Tween following which membranes were treated with Clarity Western ECL substrate (Bio-Rad) and imaged. Samples from different time points were run on the same gel to ensure identical exposure conditions. In the first set of experiments, the chemiluminescent signal intensity was normalised to the relative quantification of the corresponding intensity of $\beta-$actin. In repeat experiments, the chemiluminescent signal intensity was normalised to quantification of total protein, calculated and volume-adjusted using Image Lab 6.0 by selection of equivalent lane segments across the blot on the total protein image. For each set of experiments, data from replicates were averaged and normalised to signal at ZT 0.

Immunohistochemistry

Following sacrifice, the heart was removed and the rear wall of the right atrium encompassing the sinus node was rapidly dissected. The preparations were immersed in optimal cutting temperature compound, rapidly frozen in liquid N_2 and stored at -80^{o}C until use. The preparations were cryosectioned in a coronal plane to a thickness of 10 μm. Slides were stained using Masson's trichrome stain and the sinus node region was identified using the sinus node artery as a landmark. Two sinus node containing slides (four sections per slide) were chosen for each animal. Frozen sections were fixed in 10% formaldehyde, permeabilised with 0.1% Triton X-100 for 30 min, blocked with 1% bovine serum albumin and incubated with anti-HCN4 raised in rabbit (Alomone Labs; 1:200). Finally, sections were incubated with Cy3-conjugated secondary antibodies raised in donkey (Alomone Labs; 1:400). Images were collected on a Zeiss LSM5 PASCAL confocal microscope with a Plan Apochromat x40/1.0 oil objective lens. The confocal settings were as follows: pinhole, 1.02 airy unit; scan speed, 1 kHz unidirectional; format 1024 ×

1024. Images were collected using the following settings: Cy3, 543 nm excitation and 640-690 nm emission. Four high power images were taken per section. HCN4 immunofluorescence was quantified using Volocity cellular imaging software and analysed by Image J. The sum pixel intensity for the HCN4-stained area was divided by the area to give a measurement of intensity per unit area.

***In vitro* ChIP**

ChIP was performed on 3T3-L1 cells (ATCC, #CL-173) using the SimpleChIP chromatin immunoprecipitation kit (CST, #9005) according to the manufacturer's instructions. Prior to cross-linking, 3T3-L1 cultures at a density of 10^4 cells/cm^2 were transfected with plasmid containing His-tagged *Bmal1* (pBMPC3; gift from Aziz Sancar, Addgene, plasmid #31367) for 48 h. Antibody directed against the His-tag (CST, #12698) was used for immunoprecipitation. DNA obtained from ChIP was analysed by qPCR using primers mapping to canonical E-box binding sites, i.e., consensus binding sites for the CLOCK::BMAL1 heterodimer. E-box binding sites on the *Hcn4* gene and in 20 kb of the 5′ flanking region were obtained using the RVISTA function within ECR browser (http://ecrbrowser.dcode.org/). Quantification of *Hcn4* E-box binding sites was conducted by, first, normalisation to the housekeeping genes *Gapdh* and *L7* (input normalisation) and, secondly, normalisation to data from 3T3-L1 cells subjected to transfection treatment without plasmid. The following PCR primers were used:

Forward primer for *Hcn4* E-box binding site A	CACCCTTGCCTTCCTTCTACTG
Reverse primer for *Hcn4* E-box binding site A	ACAAAGAAAGACTCTTAGTGTGCAGGT
Forward primer for *Hcn4* E-box binding site B	GGGCTCTACCACCTCCCAG
Reverse primer for *Hcn4* E-box binding site B	GTCTGTGGGCAGGTCCATG
Forward primer for *Hcn4* E-box binding site C	GGCCATCTCTTCTCTGTGTCTGT
Reverse primer for *Hcn4* E-box binding site C	TAAGTATGAACTTCAAACGGCCAA
Forward primer for *Hcn4* E-box binding site D	GGGCTCACAAAACATGGCA
Reverse primer for *Hcn4* E-box binding site D	CCCACCAGAGCCTAGACCC
Forward primer for *Hcn4* E-box binding site E	GGCCTGATAATTGTACTGGTGGT
Reverse primer for *Hcn4* E-box binding site E	GCATTAGCCAGCCCTGTTATG
Forward primer for *Hcn4* E-box binding site F	GCCAGGTACCTGGCTTCC
Reverse primer for *Hcn4* E-box binding site F	GAACAAAGACTCAAGTACCACTCCC
Forward primer for *Hcn4* E-box binding site G	TAGCCAGGGCCTGAGGC
Reverse primer for *Hcn4* E-box binding site G	GCATGGAATGCACGGGTAG
Forward primer for *Hcn4* E-box binding site H	CCTGAAGGTCCCGTTCTTGT
Reverse primer for *Hcn4* E-box binding site H	CAGTGACAGATTGGCTTGCC
Forward primer for *Gapdh*	CTTCCGTGTTCCTACCC
Reverse primer for *Gapdh*	ACCTGGTCCTCAGTGTAGCC
Forward primer for *L7*	GAAGCTCATCTATGAGAAGGC
Reverse primer for *L7*	AAGACGAAGGAGCTGCAGAAC

Statistical analysis

To analyse circadian rhythms, data were fitted with a standard sine wave using the least-squares method using GraphPad Prism version 7. The goodness of fit as represented by R^2 (the proportion of the variance in the dependent variable that is predictable from the independent variable, in this case zeitgeber time) is reported. Significant differences (*P<0.05) between data at different zeitgeber times and/or genotypes were detected by a t test, ANOVA or limma test. Details of tests for each figure:

Figure 1A: R^2: 0.41, 0.64, 0.27, 0.48 and 0.33 (from top to bottom).
Figure 1C: Two-way ANOVA with Tukey's multiple comparisons test; *P<0.05 for ZT 12 versus ZT 0
Figure 1D: Two-tailed unpaired t test
Figure 1E: Two-way ANOVA with Sidak's test; *P<0.05 for ZT 12 versus ZT 0

Figure 2A: Limma test followed by Benjamini-Hochberg False Discovery Rate correction (set at 5%)
Figure 2B: R^2, 0.30; one-way ANOVA followed by Tukey's multiple comparisons test; ZT 6 significantly different from ZT 18

Fig 3B: Two-way ANOVA with Tukey's multiple comparisons test
Fig 3C-E: One-way ANOVA with Tukey's multiple comparisons test
Figure 3F: One-way ANOVA; no significant differences

Figure 4B,D: Two-way ANOVA with Tukey's multiple comparisons test; *P<0.05 for ZT 12 versus ZT 0

Figure 5A: Limma test followed by Benjamini-Hochberg False Discovery Rate correction (set at 5%)
Figure 5B, top panel: R2, 0.34; one-way ANOVA followed by Tukey's multiple comparisons test; ZT 0 significantly different from ZT 6, 12 and 18
Figure 5B, bottom panel: R2, 0.39; one-way ANOVA followed by Tukey's multiple comparisons test; ZT 0 significantly different from ZT 12

Figure 6A-E: Two-way ANOVA with Tukey's multiple comparisons test; *P<0.05 for ZT 12 versus ZT 0
Figure 6F: Two-way ANOVA with Holm-Šídák test; *P<0.05 for ZT 12 versus ZT 0
Figure 6H: One-way ANOVA with Dunnett's test; *P<0.05 for binding site of interest versus binding site A

SUPPLEMENTAL RESULTS

Use of a Mixed Effects Linear Model to investigate whether the circadian rhythm in heart rate is an indirect consequence of time-of-day differences in physical activity

For each animal fitted with a telemetry system, during 72 h of continuous recording in a normal light:dark cycle (Figure 1A), the heart rate and physical activity were averaged for each 5 min period. For ZT 0 - ZT 12 (*Day*) and ZT 12 - ZT 0 (*Night*), the individual activity data were then binned into *No Activity* (0 arbitrary units, au) and *High Activity* (20-30 au) groups and the corresponding heart rate recorded. A mixed effects linear model was used to analyse the data. Residual diagnostics were examined to confirm that the assumptions for the analysis to be valid were applicable. The model contains two fixed factors: *Time* (either *Day* or *Night*) and *Activity* (either *No Activity* or *High* Activity). Also included in the model was the interaction between these two factors to determine whether they were dependent on one another. The individual animal was included as a random effect. Comparisons were conducted between day and night at each of the activity levels, using a 2-sided 5% test, and applying a Sidak multiple comparison adjustment.
The following results were obtained:

Type 3 Tests of Fixed Effects				
Effect	**Degrees of freedom**	**Denominator degrees of freedom**	**F value**	**P value**
Time	1	21	9.00	0.0068
Activity	1	21	221.06	<0.0001
*Time*Activity*	1	21	1.29	0.2687

Activity	Time	Mean (beats/min)	Standard error (beats/min)	Difference (Night-Day) (beats/min)	P value
No Activity	*Day*	413.4	18.9		
	Night	451.5	18.9	38.1	0.032
High Activity	*Day*	560.9	18.9		
	Night	578	18.9	17.2	0.594

As expected, these data show that heart rates were significantly higher at night (P<0.0068) and with increased activity levels (P<0.001). However, the interaction between time and activity was not significant (P=0.2687), which means that in this dataset the heart rate difference between night and day does not depend upon activity level. Sidak's multiple comparisons test revealed a significant difference in the heart rate at *Night* versus *Day* in the *No Activity* group. In the *High Activity* group, this effect was masked (P>0.05).

SUPPLEMENTAL DISCUSSION

Use of atropine and propranolol to block the autonomic nervous system

Atropine and propranolol are commonly used to block autonomic receptors in the heart.[16] In this study, we used 1 mg/kg atropine and 1 mg/kg propranolol, as we did in our previous studies.[11] In recent studies of the mouse, Backx and colleagues[17, 18] used higher concentrations: 2 mg/kg atropine and 10 mg/kg propranolol. Propranolol blocks β-receptors with an IC_{50} of 12 nM (http://www.selleckchem.com/products/propranolol-hcl.html). In addition, work on heterologously expressed ion channels in cell lines has shown that propranolol blocks the cardiac Na^+ channel, $Na_v1.5$ (*Scn5a*), with an IC_{50} of 2.7 μM [19] and HCN4 with an IC_{50} of 50.5 μM.[20] To determine whether the non-specific effects of propranolol are a concern, we estimated the plasma propranolol concentration: assuming that only 10% of propranolol is free,[21] an injection of 10 mg/kg propranolol (as used by Backx and colleagues[17, 18]) is estimated to give a propranolol concentration of 6 μM if it partitions in all body water - ~60% of body mass in the mouse[22] - and 66 μM if it only partitions into the blood - 58.5 ml/kg in the mouse (https://www.nc3rs.org.uk/mouse-decision-tree-blood-sampling). Based on these estimates, it is possible that 10 mg/kg propranolol may block, to some extent, $Na_v1.5$ and HCN4. Because of this concern, we used a 10× lower dose of propranolol (1 mg/kg) than that used by Backx and colleagues,[17, 18] i.e. the same dose as we used before;[11] this dose is expected to cause less block of $Na_v1.5$ and little or no block of HCN4 and yet complete block of β-receptors. Atropine blocks M2 muscarinic receptors with an IC_{50} of 0.76–1.5 nM.[23-25] The dose of atropine used (1 mg/kg) is expected to cause complete block of the cardiac M2 muscarinic receptor.

Use of Cs^+ and ivabradine as I_f blockers

2 mM Cs^+ was used as an I_f blocker in experiments on the isolated sinus node. Cs^+ is a voltage-dependent blocker of I_f and block is reduced at more positive potentials.[26] Nevertheless, in rabbit sinus node cells, 2 mM Cs^+ completely blocks I_f in the pacemaker range of potentials.[27, 28] This concentration of Cs^+ has a negligible effect on the L-type Ca^{2+} current, $I_{Ca,L}$, and the delayed rectifier K^+ current,[27, 28] two currents which play a major role in the sinus node action potential.[29, 30] Cs^+ does block the background inward rectifier K^+ current, $I_{K,1}$. Isenberg[31] used 20 mM Cs^+ to block $I_{K,1}$ in sheep Purkinje fibres. It is unclear from the literature what fraction of $I_{K,1}$ will be blocked by 2 mM Cs^+. Harvey and Ten Eick[32] studied block of $I_{K,1}$ by Cs^+ in cat ventricular myocytes and reported that 1 mM Cs^+ blocked ~42% of the current at -100 mV. However, Cs^+ block of $I_{K,1}$ is voltage-dependent[32] and less block is expected in the pacemaker range of potentials. Furthermore, $I_{K,1}$ is not believed to play an important role in the centre of the sinus node (of the rabbit at least).[29, 30] We have previously discussed the use of 2 mM Cs^+ as an I_f blocker.[33] Ivabradine was used as an I_f blocker in experiments *in vivo* – Cs^+ cannot be used *in vivo*. Ivabradine is not necessarily a selective I_f blocker. 10 μM ivabradine has been reported to decrease $I_{Ca,L}$ by 18% in rabbit sinus node cells[34]; see also Haechl *et al.*[35] Ivabradine blocks heterologously expressed $Na_v1.5$ channels with an IC_{50} of 30 μM[35] and Kv11.1 (hERG) channels (responsible for the important repolarizing current $I_{K,r}$ in the sinus node) with an IC_{50} of 2-3 μM[36] or 11 μM.[35] To minimise non-specific effects

of ivabradine, it is advisable not to apply more than 3 μM ivabradine and yet at this concentration it may only block ~50% of I_f; the IC_{50} for block of I_f is reported to be 2.8 μM.[34] Ivabradine is also a use-dependent blocker and therefore requires repetitive depolarization to act.[37] Finally, block of I_f may indirectly alter intracellular Na^+[38] and therefore Ca^{2+} and this may affect pacemaking. Indeed, slowing of pacemaker activity induced by ivabradine has been shown to reduce diastolic ryanodine-receptor dependent Ca^{2+} release.[39] Therefore we cannot exclude the possibility that other components of the pacemaker mechanism beside I_f, including the Na^+/Ca^{2+} exchanger, contribute to the effect of ivabradine and to the circadian rhythm. It is concluded that neither blocker of I_f is perfect. However, in the absence of an alternative, we argue that their use is justified because it provides experimental data on the role of I_f, which is not available by any other means. When using isolated sinus node tissue, 2 mM Cs^+ is the I_f blocker of choice, because it blocks all I_f and has minimal non-specific effects. However, *in vivo* ivabradine is the only option. Both Cs^+ and ivabradine are widely used to block I_f to estimate the role of I_f in pacemaking.[e.g.11, 40-44]

Phasing of the circadian clock, *Hcn4*, HCN4 and I_f

As summarised in Supplemental Table 1, *Bmal1* (and *Clock*) peak at ~ZT 0, whereas *Hcn4* mRNA and HCN4 protein peak after a delay at ~ZT 20. Study of mouse liver cistromes has established that although CLOCK::BMAL1 binds synchronously to all of its target genes, its transcriptional output is highly heterogeneous and a large fraction of rhythmically expressed target genes are transcribed antiphase to maximal CLOCK::BMAL1 DNA binding.[45] Furthermore, a recent study has demonstrated that the mechanisms by which CLOCK::BMAL1 regulates transcription of core clock genes (such as *Per1* and Dbp) differs from the regulation of other clock-controlled genes, and that in the latter case additional mechanisms (e.g. ubiquitously expressed transcription factors) are also required for the activation of rhythmic gene expression by the circadian clock.[46] The time of the peak I_f was not determined, but the nadir in *Hcn4* mRNA, HCN4 protein and I_f was approximately the same (~ZT 6; Figs. 2B and 3C,D), suggesting that there was little delay between transcription, translation and function.

Limitations of the study

This study focussed on the potential role of a circadian rhythm in HCN4 and I_f in the sinus node, because previous work has demonstrated their importance for pacemaker function under physiological (e.g. exercise training, ageing, pregnancy and development[11, 47-50]) and pathophysiological (e.g. heart failure, atrial fibrillation, diabetes[51-54]) conditions. However, because the activity of ion channels and the rate of diastolic depolarization are coupled to intracellular Ca^{2+} release and cycling (referred to as the coupled-clock[55]), it is likely that the circadian rhythm in pacemaking involves regulation of the coupled-clock pacemaker mechanism as a whole. It was not within the scope of this study to address the functional consequences of all coupled clock molecules that showed a transcriptional day-night rhythm.

Computer modelling has the potential to show the effects of any circadian changes in ionic currents. Calculations were carried out using two independent models of the mouse sinus node action potential.[56, 57] The models suggest that a two-fold or three-fold increase in the conductance of I_f (c.f. Figure 3C) will increase the beating rate by 12 and 13 beats/min (Kharche *et al.*[57]) and by 26 and 40 beats/min (Christel *et al.*[56]). The models therefore predict a substantial change, which would at least contribute to the circadian rhythm in heart rate. Although other ionic currents could be involved, for these protein expression or corresponding current density have not been determined (only transcript expression) and, therefore, a study of the involvement of other ionic currents is premature at this stage.

In this study, one of the ways of testing the role of the vagus in setting the day-night rhythm in heart rate was by genetic ablation of $I_{K,ACh}$. However, the vagus not only lowers the heart rate by activating $I_{K,ACh}$ – it also potentially lowers the heart rate by reduction of adenylyl cyclase activity and consequent reduction of cAMP levels and protein kinase A (PKA)-dependent phosphorylation of target proteins.[e.g.58] Addressing these mechanisms is outside the scope of this work. However, it is important to note that mice carrying genetic ablation of $I_{K,ACh}$ (*Girk*$4^{-/-}$ i.e. Kir3.$4^{-/-}$) lack 50% of vagal regulation of heart rate.[9, 59] The relevance of $I_{K,ACh}$ in tonic vagal control of pacemaking is underscored by the moderate increase in basal heart rate and the delay in basal heart rate

recovery following exercise in *Girk4*$^{-/-}$ mice.[9] Mirroring the impact of $I_{K,ACh}$ ablation *in vivo*, the cholinergic negative chronotropic effect is reduced by over 50% in intact hearts and in spontaneously beating sinus node pacemaker cells isolated from *Girk4*$^{-/-}$ mice.[9] Other work from us and others has also shown the importance of $I_{K,ACh}$ in the cholinergic negative chronotropic effect as compared to any effect mediated by the cAMP/PKA-dependent pathway.[60-62].

Further studies with improved temporal resolution are also required to understand why mice with cardiac-specific *Bmal1* knockout[63, 64] or *Clock* mutant[65] retain a (albeit altered) circadian rhythm in heart rate *in vivo*. *Bmal1* and *Clock* have paralogs, *Bmal2* and *Npas2*, which can substitute for them, and this could be a potential underlying mechanism.[66, 67]

Finally, this study was carried out on mouse and rat and thus caution must be exercised in extrapolating the findings to human physiology. Although the potential for experiments on the human heart is limited, the effect of acute autonomic blockade *in vivo* would show whether the circadian rhythm in heart rate in the human is solely determined by conductance changes mediated by the autonomic nervous system.

ACKNOWLEDGEMENTS

We thank Dr. Kevin Wickman (University of Minnesota, USA), for sharing *Girk4*$^{-/-}$ mice and the *Réseau d'Animaleries de Montpellier* (RAM) for the management of *Girk4*$^{-/-}$ and corresponding wild-type mice.

ACKNOWLEDGEMENT OF FINANCIAL SUPPORT: FUNDING SOURCES

Work was supported by a British Heart Foundation Intermediate Basic Science Research Fellowship awarded to Alicia D'Souza (FS/19/1/34035), grants from the British Heart Foundation (RG/11/18/29257; PG/15/16/31330) to Mark Boyett, Halina Dobrzynski and Alicia D'Souza, and grants from the CARIPLO Foundation (ACROSS 2014-0728) and Fondation Leducq (TNE FANTASY 19CV03) awarded to Dario DiFrancesco, Mark Boyett, Halina Dobrzynski and Matteo Mangoni. Cheryl Petit was funded by a grant from the Biotechnology and Biological Sciences Research Council (BB/J003441) awarded to Hugh Piggins.

SUPPLEMENTAL REFERENCES

1. van der Horst GT, Muijtjens M, Kobayashi K, et al. Mammalian Cry1 and Cry2 are essential for maintenance of circadian rhythms. Nature 1999;398:627-630.

2. Yamaguchi S, Mitsui S, Miyake S, Yan L, Onishi H, Yagita K, Suzuki M, Shibata S, Kobayashi M, Okamura H. The 5' upstream region of mPer1 gene contains two promoters and is responsible for circadian oscillation. Current Biology 2000;10:873-876.

3. Sakhi K, Wegner S, Belle MD, Howarth M, Delagrange P, Brown TM, Piggins HD. Intrinsic and extrinsic cues regulate the daily profile of mouse lateral habenula neuronal activity. Journal of Physiology 2014;592:5025-5045.

4. Wickman K, Nemec J, Gendler SJ, Clapham DE. Abnormal heart rate regulation in GIRK4 knockout mice. Neuron 1998;20:103-114.

5. Gibbs J, Ince L, Matthews L, et al. An epithelial circadian clock controls pulmonary inflammation and glucocorticoid action. Nature Medicine 2014;20:919-926.

6. Agah R, Frenkel PA, French BA, Michael LH, Overbeek PA, Schneider MD. Gene recombination in postmitotic cells. Targeted expression of Cre recombinase provokes cardiac-restricted, site-specific rearrangement in adult ventricular muscle in vivo. Journal of Clinical Investigation 1997;100:169-179.

7. Zhang Y, Wu J, King JH, Huang CL, Fraser JA. Measurement and interpretation of electrocardiographic QT intervals in murine hearts. American Journal of Physiology: Heart and Circulatory Physiology 2014;306:H1553-1557.

8. Boukens BJ, Rivaud MR, Rentschler S, Coronel R. Misinterpretation of the mouse ECG: 'musing the waves of Mus musculus'. Journal of Physiology 2014;592:4613-4626.

9. Mesirca P, Marger L, Toyoda F, et al. The G-protein-gated K^+ channel, I_{KACh}, is required for regulation of pacemaker activity and recovery of resting heart rate after sympathetic stimulation. Journal of General Physiology 2013;142:113-126.

10. Baruscotti M, Bucchi A, Viscomi C, Mandelli G, Consalez G, Gnecchi-Rusconi T, Montano N, Casali KR, Micheloni S, Barbuti A, DiFrancesco D. Deep bradycardia and heart block caused by inducible cardiac-specific knockout of the pacemaker channel gene Hcn4.

Proceedings of the National Academy of Sciences of the United States of America 2011;108:1705-1710.
11. D'Souza A, Bucchi A, Johnsen AB, et al. Exercise training reduces resting heart rate via downregulation of the funny channel HCN4. Nature Communications 2014;5:3775.
12. Lin H, Xiao J, Luo X, Chen G, Wang Z. Transcriptional control of pacemaker channel genes HCN2 and HCN4 by Sp1 and implications in re-expression of these genes in hypertrophied myocytes. Cellular Physiology and Biochemistry 2009;23:317-326.
13. Lowe M, Lage J, Paatela E, et al. Cry2 Is critical for circadian regulation of myogenic differentiation by Bclaf1-mediated mRNA stabilization of cyclin D1 and Tmem176b. Cell Reports 2018;22:2118-2132.
14. Hughes ME, Hogenesch JB, Kornacker K. JTK_CYCLE: an efficient nonparametric algorithm for detecting rhythmic components in genome-scale data sets. Journal of Biological Rhythms 2010;25:372-380.
15. Guilding C, Hughes AT, Brown TM, Namvar S, Piggins HD. A riot of rhythms: neuronal and glial circadian oscillators in the mediobasal hypothalamus. Molecular Brain 2009;2:28.
16. Boyett MR, D'Souza A, Zhang H, Morris GM, Dobrzynski H, Monfredi O. Viewpoint: Is the resting bradycardia in athletes the result of remodelling of the sinoatrial node rather than high vagal tone? Journal of Applied Physiology 2013;114:1351-1355.
17. Aschar-Sobbi R, Izaddoustdar F, Korogyi AS, et al. Increased atrial arrhythmia susceptibility induced by intense endurance exercise in mice requires TNF∝. Nature Communications 2015;6:6018.
18. Lakin R, Guzman C, Izaddoustdar F, Polidovitch N, Goodman JM, Backx PH. Changes in heart rate and its regulation by the autonomic nervous system do not differ between forced and voluntary exercise in mice. Frontiers in Physiology 2018;9.
19. Wang DW, Mistry AM, Kahlig KM, Kearney JA, Xiang J, George AL, Jr. Propranolol blocks cardiac and neuronal voltage-gated sodium channels. Frontiers in Pharmacology 2010;1:144.
20. Tamura A, Ogura T, Uemura H, Reien Y, Kishimoto T, Nagai T, Komuro I, Miyazaki M, Nakaya H. Effects of antiarrhythmic drugs on the hyperpolarization-activated cyclic nucleotide-gated channel current. Journal of Pharmacological Sciences 2009;110:150-159.
21. Taylor EA, Turner P. The distribution of propranolol, pindolol and atenolol between human erythrocytes and plasma. British Journal of Clinical Pharmacology 1981;12:543-548.
22. Chapman ME, Hu L, Plato CF, Kohan DE. Bioimpedance spectroscopy for the estimation of body fluid volumes in mice. American Journal of Physiology - Renal Physiology 2010;299:F280-283.
23. Moriya H, Takagi Y, Nakanishi T, Hayashi M, Tani T, Hirotsu I. Affinity profiles of various muscarinic antagonists for cloned human muscarinic acetylcholine receptor (mAChR) subtypes and mAChRs in rat heart and submandibular gland. Life Sciences 1999;64:2351-2358.
24. Buckley NJ, Bonner TI, Buckley CM, Brann MR. Antagonist binding properties of five cloned muscarinic receptors expressed in CHO-K1 cells. Molecular Pharmacology 1989;35:469.
25. Bolden C, Cusack B, Richelson E. Antagonism by antimuscarinic and neuroleptic compounds at the five cloned human muscarinic cholinergic receptors expressed in Chinese hamster ovary cells. Journal of Pharmacology and Experimental Therapeutics 1992;260:576-580.
26. DiFrancesco D. Block and activation of the pace-maker channel in calf Purkinje fibres: effects of potassium, caesium and rubidium. Journal of Physiology 1982;329:485-507.
27. Liu YM, Yu H, Li C-Z, Cohen IS, Vassalle M. Cesium effects on i_f and i_K in rabbit sinoatrial node myocytes: implications for SA node automaticity. Journal of Cardiovascular Pharmacology 1998;32:783-790.
28. Denyer JC, Brown HF. Pacemaking in rabbit isolated sino-atrial node cells during Cs^+ block of the hyperpolarization-activated current i_f. Journal of Physiology 1990;429:401-409.
29. Brown HF. Electrophysiology of the sinoatrial node. Physiological Reviews 1982;62:505-530.

30. Zhang H, Holden AV, Kodama I, Honjo H, Lei M, Varghese T, Boyett MR. Mathematical models of action potentials in the periphery and center of the rabbit sinoatrial node. American Journal of Physiology 2000;279:H397-H421.

31. Isenberg G. Cardiac Purkinje fibers: cesium as a tool to block inward rectifying potassium currents. Pflugers Archiv 1976;365:99-106.

32. Harvey RD, Ten Eick RE. Voltage-dependent block of cardiac inward-rectifying potassium current by monovalent cations. Journal of General Physiology 1989;94:349-361.

33. Nikmaram MR, Boyett MR, Kodama I, Suzuki R, Honjo H. Variation in the effects of Cs^+, UL-FS 49 and ZD7288 within the sinoatrial node. American Journal of Physiology 1997;272:H2782-H2792.

34. Bois P, Bescond J, Renaudon B, Lenfant J. Mode of action of bradycardic agent, S 16257, on ionic currents of rabbit sinoatrial node cells. British Journal of Pharmacology 1996;118:1051-1057.

35. Haechl N, Ebner J, Hilber K, Todt H, Koenig X. Pharmacological profile of the bradycardic agent ivabradine on human cardiac ion channels. Cellular Physiology and Biochemistry 2019;53:36-48.

36. Melgari D, Brack KE, Zhang C, Zhang Y, Harchi AE, Mitcheson JS, Dempsey CE, Ng GA, Hancox JC. hERG potassium channel blockade by the HCN channel inhibitor bradycardic agent ivabradine. J Am Heart Assoc 2015;4:e001813.

37. Bucchi A, Tognati A, Milanesi R, Baruscotti M, DiFrancesco D. Properties of ivabradine-induced block of HCN1 and HCN4 pacemaker channels. Journal of Physiology 2006;572:335-346.

38. Boyett MR, Hart G, Levi AJ. Factors affecting intracellular sodium during repetitive activity in isolated sheep Purkinje fibres. Journal of Physiology 1987;384:405-429.

39. Yaniv Y, Sirenko S, Ziman BD, Spurgeon HA, Maltsev VA, Lakatta EG. New evidence for coupled clock regulation of the normal automaticity of sinoatrial nodal pacemaker cells: bradycardic effects of ivabradine are linked to suppression of intracellular Ca^{2+} cycling. Journal of Molecular and Cellular Cardiology 2013;62:80-89.

40. Verkerk AO, Wilders R, van Borren MM, Peters RJ, Broekhuis E, Lam K, Coronel R, de Bakker JM, Tan HL. Pacemaker current (I_f) in the human sinoatrial node. European Heart Journal 2007;28:2472-2478.

41. Noma A, Morad M, Irisawa H. Does the "pacemaker current" generate the diastolic depolarization in the rabbit SA node cells? Pflugers Archiv 1983;397:190-194.

42. Zhou Z, Lipsius SL. Properties of the pacemaker current (I_f) in latent pacemaker cells isolated from cat right atrium. Journal of Physiology 1992;453:503-523.

43. Sosunov EA, Anyukhovsky EP. Differential effects of ivabradine and ryanodine on pacemaker activity in canine sinus node and Purkinje fibers. Journal of Cardiovascular Electrophysiology 2012;23:650-655.

44. DiFrancesco D. The role of the funny current in pacemaker activity. Circulation Research 2010;106:434-446.

45. Menet JS, Rodriguez J, Abruzzi KC, Rosbash M. Nascent-Seq reveals novel features of mouse circadian transcriptional regulation. Elife 2012;1:e00011.

46. Trott AJ, Menet JS. Regulation of circadian clock transcriptional output by CLOCK:BMAL1. PLoS Genetics 2018;14:e1007156.

47. Larson ED, St Clair JR, Sumner WA, Bannister RA, Proenza C. Depressed pacemaker activity of sinoatrial node myocytes contributes to the age-dependent decline in maximum heart rate. Proceedings of the National Academy of Sciences of the United States of America 2013;110:18011-18016.

48. El Khoury N, Mathieu S, Marger L, Ross J, El Gebeily G, Ethier N, Fiset C. Upregulation of the hyperpolarization-activated current increases pacemaker activity of the sinoatrial node and heart rate during pregnancy in mice. Circulation 2013;127:2009-2020.

49. Abd Allah ESH, Tellez JO, Nelson T, Monfredi O, Boyett MR, Dobrzynski H. Changes in the expression of ion channels, connexins and Ca^{2+}-handling proteins in the sinoatrial node during postnatal development. Experimental Physiology 2011;96:426-438.

50. D'Souza A, Pearman CM, Wang Y, et al. Targeting miR-423-5p reverses exercise training-induced HCN4 channel remodeling and sinus bradycardia. Circulation Research 2017;121:1058-1068.

51. Yeh YH, Burstein B, Qi XY, Sakabe M, Chartier D, Comtois P, Wang Z, Kuo CT, Nattel S. Funny current downregulation and sinus node dysfunction associated with atrial tachyarrhythmia: a molecular basis for tachycardia-bradycardia syndrome. Circulation 2009;119:1576-1585.

52. Zicha S, Fernandez-Velasco M, Lonardo G, L'Heureux N, Nattel S. Sinus node dysfunction and hyperpolarization-activated (HCN) channel subunit remodeling in a canine heart failure model. Cardiovascular Research 2005;66:472-481.

53. Zhang Y, Wang Y, Yanni J, Qureshi MA, Logantha S, Kassab S, Boyett MR, Gardiner NJ, Sun H, Howarth FC, Dobrzynski H. Electrical conduction system remodeling in streptozotocin-induced diabetes mellitus rat heart. Frontiers in Physiology 2019;10:826.

54. Yanni J, D'Souza A, Wang Y, et al. Silencing miR-370-3p rescues funny current and sinus node function in heart failure. Scientific Reports 2020;10:11279.

55. Lyashkov AE, Behar J, Lakatta EG, Yaniv Y, Maltsev VA. Positive feedback mechanisms among local Ca releases, NCX, and I_{CaL} ignite pacemaker action potentials. Biophysical Journal 2018;114:2024-2024.

56. Christel CJ, Cardona N, Mesirca P, Herrmann S, Hofmann F, Striessnig J, Ludwig A, Mangoni ME, Lee A. Distinct localization and modulation of Cav1.2 and Cav1.3 L-type Ca^{2+} channels in mouse sinoatrial node. Journal of Physiology 2012;590:6327-6342.

57. Kharche S, Yu J, Lei M, Zhang H. A mathematical model of action potentials of mouse sinoatrial node cells with molecular bases. American Journal of Physiology 2011;301:H945-963.

58. Lakatta EG. A paradigm shift for the heart's pacemaker. Heart Rhythm 2010;7:559-564.

59. Wickman K, Nemec J, Gendler SJ, Clapham DE. Abnormal heart rate regulation in GIRK4 knockout mice. Neuron 1998;20:103-114.

60. Zhang H, Holden AV, Noble D, Boyett MR. Analysis of the chronotropic effect of acetylcholine on sinoatrial node cells. Journal of Cardiovascular Electrophysiology 2002;13:465-474.

61. Boyett MR, Kodama I, Honjo H, Arai A, Suzuki R, Toyama J. Ionic basis of the chronotropic effect of acetylcholine on the rabbit sinoatrial node. Cardiovascular Research 1995;29:867-878.

62. Lyashkov AE, Vinogradova TM, Zahanich I, Li Y, Younes A, Nuss HB, Spurgeon HA, Maltsev VA, Lakatta EG. Cholinergic receptor signaling modulates spontaneous firing of sinoatrial nodal cells via integrated effects on PKA-dependent Ca^{2+} cycling and I_{KACh}. American Journal of Physiology: Heart and Circulatory Physiology 2009;297:H949-959.

63. Schroder EA, Lefta M, Zhang X, Bartos DC, Feng HZ, Zhao Y, Patwardhan A, Jin JP, Esser KA, Delisle BP. The cardiomyocyte molecular clock, regulation of Scn5a, and arrhythmia susceptibility. American Journal of Physiology-Cell Physiology 2013;304:C954-965.

64. Schroder EA, Burgess DE, Zhang X, Lefta M, Smith JL, Patwardhan A, Bartos DC, Elayi CS, Esser KA, Delisle BP. The cardiomyocyte molecular clock regulates the circadian expression of Kcnh2 and contributes to ventricular repolarization. Heart Rhythm 2015;12:1306-1314.

65. Bray MS, Shaw CA, Moore MW, et al. Disruption of the circadian clock within the cardiomyocyte influences myocardial contractile function, metabolism, and gene expression. American Journal of Physiology-Heart and Circulatory Physiology 2008;294:H1036-1047.

66. Shi S, Hida A, McGuinness OP, Wasserman DH, Yamazaki S, Johnson CH. Circadian clock gene Bmal1 is not essential; functional replacement with its paralog, Bmal2. Current Biology 2010;20:316-321.

67. Landgraf D, Wang LL, Diemer T, Welsh DK. NPAS2 compensates for loss of CLOCK in peripheral circadian oscillators. PLoS Genetics 2016;12:e1005882.

Supplemental Table 1. Summary of circadian rhythms in heart rate, *Bmal1*, *Clock* and *Hcn4*. Where possible the data were calculated from the fitting of a sine wave. The periodicity was assumed to be 24 h. [a]data based on a small number of time points over 24 h and, therefore, subject to greater error. [b]data based on means at ZT 0 and ZT 12 and, therefore, no time course data available. Data are ranked according to the likely sequence of events.

Event	Source data	Day-night difference in heart rate (beats/min)	Time of peak (ZT)	Timeline
Early events				
Bmal1 mRNA[a]	Figure 5B	-	0.5±1.1	**Clock**
Clock mRNA[a]	Figure 5B	-	0.2±1.0	
Later events				***Hcn4***
Hcn4 mRNA[a]	Figure 2B	-	19.7±1.0	
Intrinsic beating rate (not subject to autonomic influence)				**Intrinsic heart rate**
Isolated sinus node – study 1[b]	Figure 1D	55±9	-	
Isolated sinus node – study 2[b]	Figure 4D	52±16	-	
Isolated sinus node after Cs^+ block of I_f – study 2[b]	Figure 4D	-5±5	-	
Isolated sinus node from *Bmal1*$^{-/-}$ mouse[b]	Figure 6C	-37±8	-	
Heart rate *in vivo* of anaesthetised mouse subject to autonomic blockade[b]	Figure 1C	28±7	-	**Normal heart rate**
Normal heart rate (subject to autonomic influence)				
Heart rate *in vivo* of conscious mouse – study 1	Figure 1A	76±4	14.1±0.1	
Heart rate *in vivo* of conscious mouse – study 2	Figure 1F	155	12.5	
Heart rate *in vivo* of conscious *Girk4*$^{-/-}$ mouse – study 2	Figure 1F	155	12.3	
Heart rate *in vivo* of conscious mouse – study 3[b]	Figure 4B	203±17	-	
Heart rate *in vivo* of conscious mouse after ivabradine block of I_f – study 3[b]	Figure 4B	-9±4	-	
Heart rate *in vivo* of anaesthetised mouse[b]	Figure 1C	54±14	-	
Normal heart rate (subject to autonomic influence) but with altered lighting regime				
Heart rate *in vivo* of conscious mouse during 24 h dark regime	Figure 1A	103±5	15.1±0.2	

Supplemental Table 2. Expression of mRNA for clock components, transcription factors, ion channels, Na^+-K^+ pump subunits, intracellular Ca^{2+}-handling molecules, gap junction channels and hypertrophy markers in the sinus node at ZT 0 and ZT 12. Values denote ΔCt (abundance of transcript normalised to reference transcripts *Tbp* and *Ipo8*) and are transformed (Efficiency$^{-\Delta Ct}$). Differences between ZT 0 and ZT 12 were tested using the limma test and the False Discovery Rate (FDR)-corrected P values are shown. Statistically significant differences (P<0.05) are highlighted in grey. n=7/9.

mRNA	Protein	ZT 0 (mean±SEM)	ZT 12 (mean±SEM)	FDR-adjusted P value
	Clock genes			
Arid1A	AT-rich interactive domain-containing protein 1A	1.29±0.25	1.59±0.11	0.301
Bhlhe40	Class E basic helix-loop-helix protein 40	0.63±0.18	1.75±0.34	0.031
Bhlhe41	Class E basic helix-loop-helix protein 41	0.95±0.10	4.35±0.79	0.001
Bmal1	Aryl hydrocarbon receptor nuclear translocator-like protein 1	0.91±0.15	0.07±0.01	1.92E-06
Bmal2	Aryl hydrocarbon receptor nuclear translocator-like protein 2	0.02±0.003	0.05±0.02	0.977
Clock	Circadian locomoter output cycles protein kaput	5.17±1.49	2.15±0.28	0.099
Cry1	Cryptochrome-1	0.51±0.05	0.40±0.04	0.298
Cry2	Cryptochrome-2	0.40±0.04	1.25±0.25	0.002
Csnk1e	Casein kinase I isoform epsilon	0.99±0.10	1.54±0.25	0.307
Lhx1	LIM/homeobox protein Lhx1	0.001±0.0003	0.001±0.0005	0.873
Per1	Period circadian protein homolog 1	0.43±0.06	1.84±0.16	2.26E-05
Per2	Period circadian protein homolog 2	0.18±0.02	0.93±0.05	5.11E-07
Per3	Period circadian protein homolog 3	0.22±0.02	1.59±0.09	1.61E-08
Nr1d1	Nuclear receptor subfamily 1 group D member 1	0.33±0.03	4.19±0.66	4.42E-08
Nr1d2	Nuclear receptor subfamily 1 group D member 2	1.88±0.73	8.22±2.75	0.005
RoRa	Nuclear receptor ROR-alpha	1.57±0.17	2.19±0.27	0.186
Timeless	Protein timeless homolog	0.15±0.01	0.19±0.01	0.271
	Circadian clock regulated transcription factors			
Dbp	D site-binding protein	0.05±0.01	3.97±0.22	4.04E-11
Hlf	Hepatic leukemia factor	2.27±0.47	4.40±0.33	0.012
Tef	Thyrotroph embryonic factor	1.42±0.13	6.57±0.50	5.11E-07

Supplemental Table 2 continued.

Gene	Protein	ZT 0 (mean±SEM)	ZT 12 (mean±SEM)	FDR adjusted P value
		HCN channels		
Hcn1	HCN1	5.01±0.75	6.34±3.07	0.620
Hcn2	HCN2	0.49±0.07	0.66±0.06	0.252
Hcn4	HCN4	12.05±1.32	6.39±1.42	0.028
		Na^+ channels		
Scn5a	$Na_v1.5$	4.17±0.45	8.08±0.83	0.005
Scn1b	$Na_v\beta.1$	2.34±0.24	3.4±0.59	0.354
		Ca^{2+} channels		
Cacna1c	$Ca_v1.2$	1.71±0.27	2.08±0.35	0.928
Cacna1d	$Ca_v1.3$	0.59±0.15	0.82±0.15	0.385
Cacna1g	$Ca_v3.1$	1.12±0.14	1.17±0.13	0.789
Cacna1h	$Ca_v3.2$	4.31±0.64	7.63±1.20	0.084
Cacna2d1	$Ca_v\alpha2\delta1$	13.21±4.71	16.20±9.22	0.873
Cacna2d2	$Ca_v\alpha2\delta2$	3.56±0.61	5±0.81	0.354
Cacnb2	$Ca_v\beta2$	1.85±0.27	4.06±0.78	0.084
		Transient outward K^+ channels		
Kcna2	$K_v1.2$	0.33±0.04	0.48±0.04	0.109
Kcna4	$K_v1.4$	0.14±0.01	0.29±0.01	0.002
Kcnb1	$K_v2.1$	1.70±0.18	1.23±0.11	0.163
Kcnd2	$K_v4.2$	0.46±0.04	1.14±0.08	2.22E-04
Kcnd3	$K_v4.3$	0.65±0.16	0.80±0.09	0.333
Kcnip2	KChIP2	0.24±0.02	0.26±0.04	0.975
		Delayed rectifier K^+ channels		
Kcna5	$K_v1.5$	0.40±0.05	0.73±0.06	0.021
Kcnh2	ERG1	1.32±0.2	3.01±0.34	0.009
Kcnq1	K_VLQT1	2.06±0.16	2.55±0.23	0.217
		Inward rectifier K^+ channels		
Kcnj2	Kir2.1	1.55±0.15	1.78±0.18	0.596
Kcnj12	Kir2.2	0.84±0.07	1.19±0.10	0.084
Kcnj4	Kir2.3	0.004±0.0009	0.008±0.002	0.466
Kcnj14	Kir2.4	0.11±0.02	0.10±0.01	0.629
Kcnj3	Kir3.1	14.19±1.83	22.31±3.75	0.117
Kcnj5	Kir3.4	7.60±0.65	10.06±0.95	0.187
Kcnj8	Kir6.1	1.02±0.06	1.63±0.15	0.031
Kcnj11	Kir6.2	1.32±0.14	2.86±0.26	0.002
Abcc8	SUR1	1.57±0.19	2.88±0.27	0.006
Abcc9	SUR2	2.23±0.33	4.67±0.26	0.002

Supplemental Table 2 continued.

mRNA	Protein	ZT 0 (mean±SEM)	ZT 12 (mean±SEM)	FDR adjusted P value
		Miscellaneous K^+ channels		
Kcnn1	SK1	0.16±0.02	0.29±0.07	0.157
Kcnn2	SK2	0.48±0.05	0.60±0.04	0.217
Kcnn3	SK3	0.08±0.01	0.10±0.01	0.328
Kcnk3	TASK1	10.68±1.36	22.69±6.21	0.033
Trpc3	TRPC3	1.85±0.04	0.12±0.01	0.489
		Cl^- channels		
Cftr	CFTR	0.06±0.01	0.05±0.004	0.819
Clcn2	CLC-2	0.08±0.01	0.30±0.04	0.001
		Na^+-K^+ Pump		
Atp1a1	Na^+-K^+ pump α1 subunit	45.33±9.48	42.64±8.96	0.983
Atp1a2	Na^+-K^+ pump α2 subunit	20.26±3.09	34.74±13.72	0.443
Atp1a3	Na^+-K^+ pump α3 subunit	0.2±0.05	0.62±0.14	0.106
		Intracellular Ca^{2+}-handling molecules		
Casq2	Calsequestrin 2	59.30±22.84	40.26±16.71	0.385
Camk2d	Camk2δ	3.04±0.37	4.92±0.45	0.046
Slc8a1	NCX1	9.30±0.49	15.28±2.76	0.179
Pln	Phospholamban	1.15±0.09	1.47±0.24	0.789
Ryr2	RYR2	63.75±24.87	70.52±37.08	0.807
Ryr3	RYR3	0.48±0.27	0.30±0.04	0.807
Sln	Sarcolipin	97.28±5.87	86.02±14.31	0.415
Atp2a2	SERCA2a	857±429.6	953.59±633.82	0.852
		Gap junction channels		
Gjd3	Cx30.2	0.06±0.01	0.08±0.01	0.367
Gja5	Cx40	1.15±0.22	2.29±0.52	0.102
Gja1	Cx43	1.95±0.22	1.488±0.26	0.247
Gjc1	Cx45	0.06±0.02	0.06±0.014	0.835

Supplemental Table 2 continued.

mRNA	Protein	ZT 0 (mean±SEM)	ZT 12 (mean±SEM)	FDR adjusted P value
		Transcription factors		
Gata4	GATA4	3.32±0.34	3.35±0.37	0.975
Hand2	Heart- and neural crest derivatives-expressed protein 2	1.21±0.1	1.72±0.17	0.136
Isl1	Insulin gene enhancer protein ISL-1	0.36±0.08	0.19±0.04	0.110
Klf4	Krueppel-like factor 4	1.64±0.23	1.40±0.07	0.593
Klf15	Krueppel-like factor 15	0.56±0.057	1.03±0.08	0.011
Mef2c	Myocyte-specific enhancer factor 2C	1.02±0.11	1.42±0.20	0.411
Nkx2.5	Homeobox protein Nkx-2.5	1.36±0.18	1.60±0.31	0.693
Rest	RE1-silencing transcription factor	0.47±0.1	0.44±0.02	0.883
Pitx2	Pituitary homeobox 2	0.14±0.03	0.12±0.01	0.620
Shox2	Short stature homeobox protein 2	0.98±0.14	0.42±0.06	0.005
Srf	Serum response factor	2.46±0.15	2.30±0.15	0.695
Tbx3	T-box transcription factor 3	1.80±0.22	0.96±0.12	0.028
Tbx5	T-box transcription factor 5	8.57±0.8	11.49±1.51	0.376
Tbx18	T-box transcription factor 18	0.78±0.14	0.41±0.06	0.063
		Hypertrophy markers		
Nppa	Atrial natriuretic peptide	114±22.17	317.57±103.9	0.032
Nppb	Brain natriuretic peptide	0.99±0.28	2.20±1.09	0.645

Supplemental Table 3. Mean delta Ct values ($Ct_{reference\ gene}/Ct_{gene\ of\ interest}$) for *Hcn4*, *Bmal1* and *Clock* and corrrsponding Ct values for the reference transcripts, *Ipo8* and *Tbp1*, in individual runs of single-assay qPCR data presented in Figures 2B and 5B. n=6/6/6/6 for *Hcn4* and n=6/6/7/8 for *Bmal1* and *Clock*.

	***Hcn4* (Figure 2B)**		
	Run 1	**Run 2**	**Average**
ZT 0	2.7±0.39	2.77±0.40	2.76±0.4
ZT 6	1.8±0.34	1.75±0.30	1.75±0.3
ZT 12	2.01±0.16	2.06±0.23	2.05±0.22
ZT 18	3.03±0.33	3.19±0.40	3.18±0.40
	***Ipo8* (Figure 2B)**		
	Run 1	**Run 2**	**Average**
ZT 0	25.95±0.20	25.98±0.12	25.96±0.14
ZT 6	26.23+0.58	26.19±0.17	26.21±0.19
ZT 12	25.78±0.23	25.85±0.06	25.81±0.07
ZT 18	27.10±0.32	27.24±0.37	27.17±0.34
	***Tbp1* (Figure 2B)**		
	Run 1	**Run 2**	**Average**
ZT 0	24.03±0.1	23.99±0.09	24.01±0.09
ZT 6	24.19±0.14	24.20±0.14	24.19±0.14
ZT 12	23.89±0.07	23.77±0.08	23.83±0.07
ZT 18	24.89±0.26	24.87±0.26	24.87±0.26

Supplemental Table 3 continued.

***Bmal1* (Fig 5B)**			
	Run 1	**Run 2**	**Average**
ZT 0	0.61±0.22	1.02±0.38	0.86±0.29
ZT 6	0.17±0.04	0.26±0.05	0.22±0.03
ZT 12	0.11±0.06	0.04±0.008	0.07±0.03
ZT 18	0.13±0.04	0.24±0.07	0.18±0.05
***Clock* (Fig 5B)**			
	Run 1	**Run 2**	**Average**
ZT 0	10.86±1.13	18.79±6.6	14.57±2.62
ZT 6	4.69±0.04	11.31±3.2	8.66±1.13
ZT 12	4.99±0.52	7.12±0.51	5.87±0.89
ZT 18	8.72±3.33	8.811±0.05	8.55±1.71
Ipo8			
	Run 1	**Run 2**	**Average**
ZT 0	25.98±0.34	24.48±0.33	25.22±0.28
ZT 6	26.81±0.92	26.62±1.05	26.25±0.61
ZT 12	25.43±0.29	24.58±0.1	25.01±0.20
ZT 18	25.8±0.26	24.99±0.18	25.39±0.22
Tbp1			
	Run 1	**Run 2**	**Average**
ZT 0	27.78±1.35	27.73±1.44	27.08±0.72
ZT 6	27.34±0.94	27.05±0.93	26.68±0.51
ZT 12	26.01±0.11	25.77±0.18	25.91±0.13
ZT 18	25.97±0.25	26.06±0.12	26±0.18

Supplemental Table 4. Mean delta Ct values ($Ct_{reference\ gene}/Ct_{gene\ of\ interest}$) for *Bmal1*, *Clock* and *Hcn4* and corrrsponding mean Ct values for the reference transcripts, *Ipo8* and *Tbp1*, in individual runs of single-assay qPCR data presented in Figures 6A,B,E. n=6/7/5/6 for *Bmal1* and *Clock* and n=6/7/5/6 for *Hcn4*.

Wild-Type				*Bmal1* Knockout			
***Bmal1* (Figure 6A)**							
	Run 1	**Run 2**	**Average**		**Run 1**	**Run 2**	**Average**
ZT 0	0.61±0.27	1.02±0.38	0.86±0.29	ZT 0	0.053±0.01	0.030±0.01	0.04±0.01
ZT 12	0.11±0.05	0.04±0.007	0.07±0.03	ZT 12	0.005±0.002	0.006±0.004	0.004±0.002
***Clock* (Figure 6B)**							
	Run 1	**Run 2**	**Average**		**Run 1**	**Run 2**	**Average**
ZT 0	10.86±1.13	18.79±6.6	14.57±2.62	ZT 0	8.2±1.35	8.85±1.76	6.8±1.30
ZT 12	4.99±0.52	7.12±0.51	5.87±0.89	ZT 12	6.8±1.06	2.98±1.96	4±0.68
***Hcn4* (Figure 6E)**							
	Run 1	**Run 2**	**Average**		**Run 1**	**Run 2**	**Average**
ZT 0	30.68±10.25	49.76±12.17	42±4.7	ZT 0	18.75±9.36	36.03±5.73	27±5.7
ZT 12	15.52±2.13	32.87±3.86	24±2.8	ZT 12	29.22±17.36	20.17±3.24	24±7.2
***Ipo8* (Figure 6)**							
	Run 1	**Run 2**	**Average**		**Run 1**	**Run 2**	**Average**
ZT 0	25.98±0.34	24.48±0.33	25.22±0.28	ZT 0	25.8±0.52	27.31±0.82	25.17±0.18
ZT 12	25.43±0.29	24.58±0.1	25.01±0.20	ZT 12	27.26±0.61	26.53±0.56	26.29±0.34
***Tbp* (Figure 6)**							
	Run 1	**Run 2**	**Average**		**Run 1**	**Run 2**	**Average**
ZT 0	27.78±1.35	27.73±1.44	27.08±0.72	ZT 0	24.8±0.21	25.44±0.15	26.33±0.3
ZT 12	26.01±0.11	25.77±0.18	25.91±0.13	ZT 12	25.28±0.47	25.74±0.18	26.01±0.32

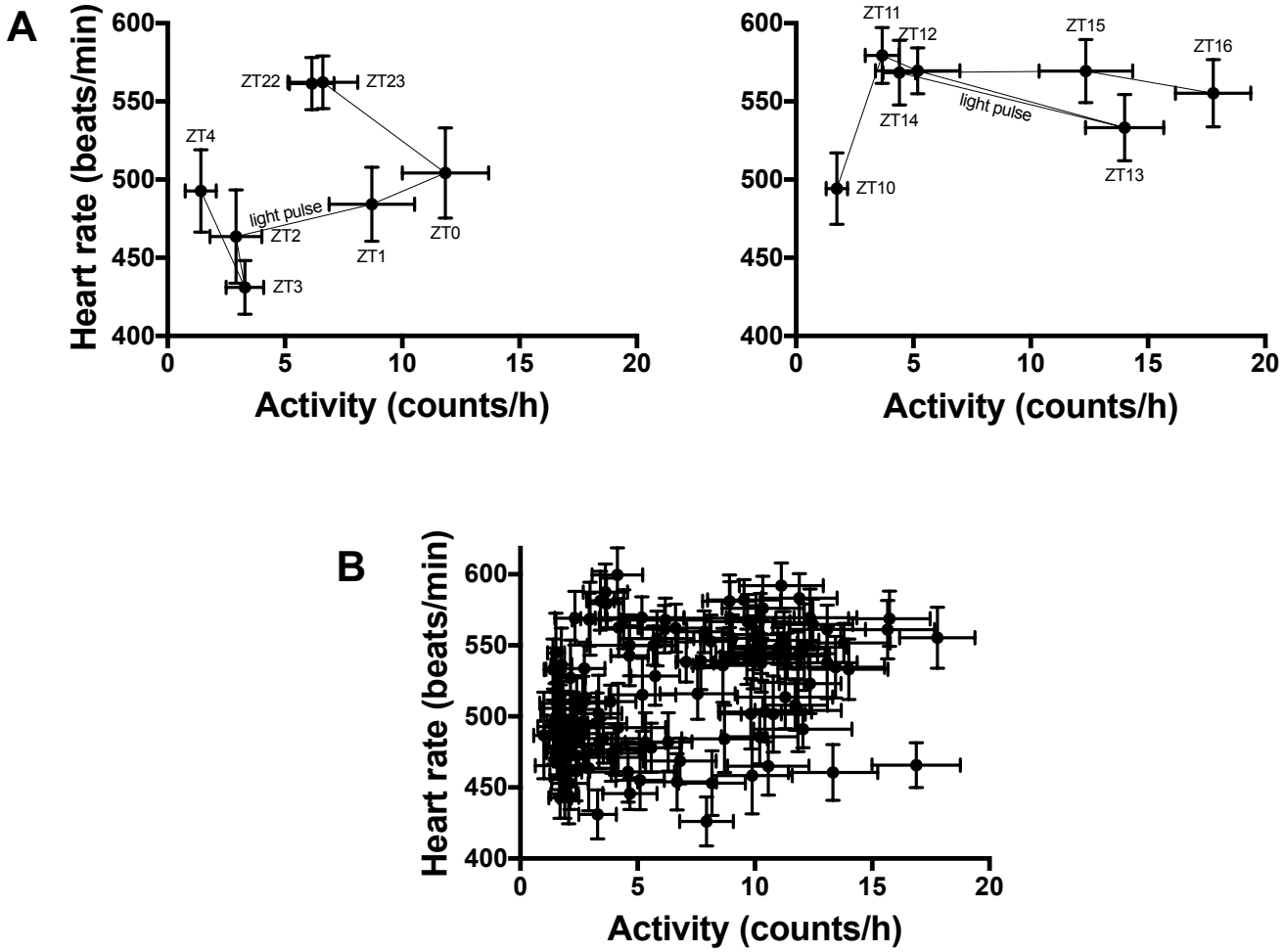

Supplemental Figure 1. A, Relationship between *in vivo* heart rate and physical activity before, during and after the 1 h light pulses shown in Figure 1B. **B**, Relationship between *in vivo* heart rate and physical activity throughout the 6-day experiment shown in Figure 1A.

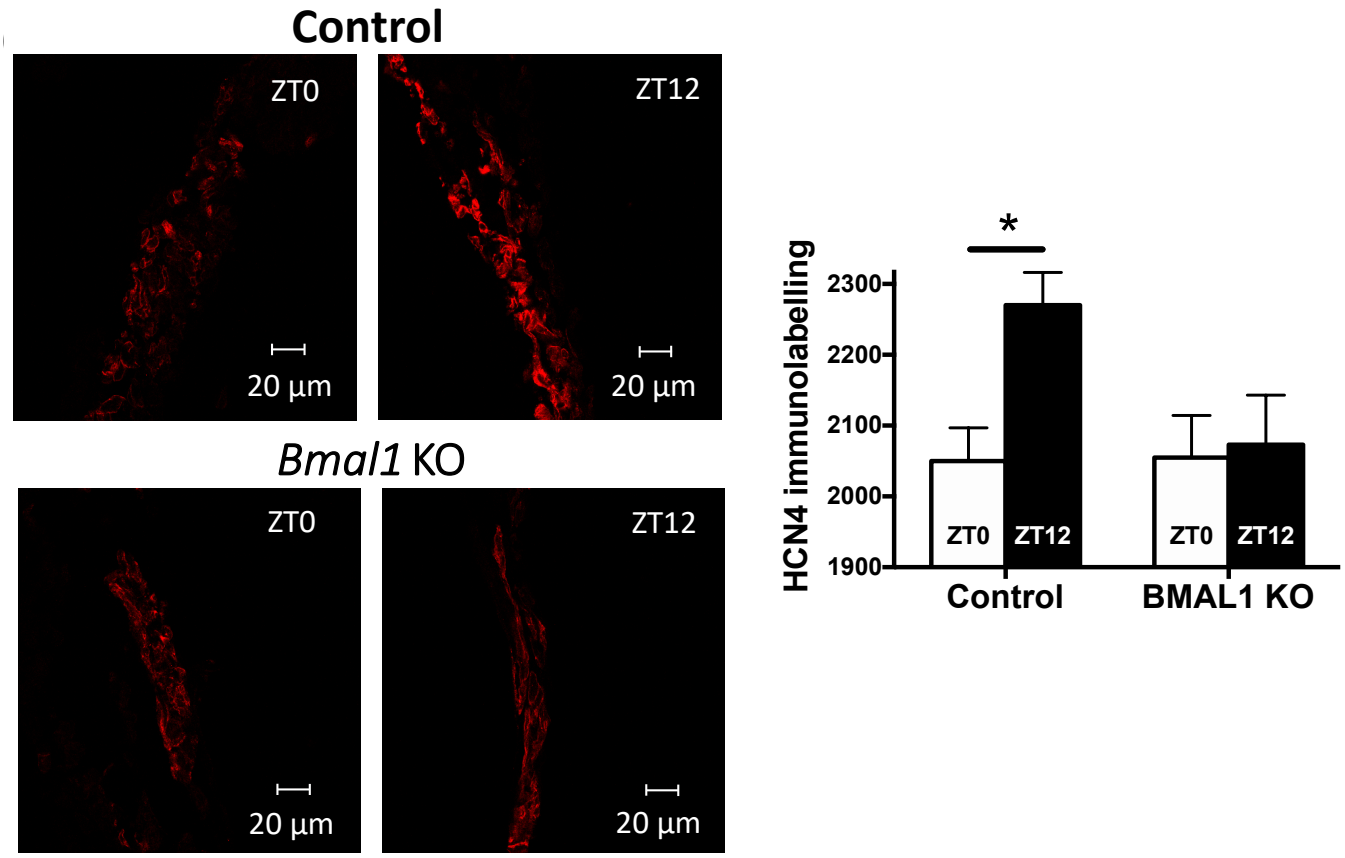

Supplemental Figure 2. Left, Immunolabelling of HCN4 protein (red signal) in sections through the sinus node dissected from control wild-type (top) and cardiac-specific *Bmal1* knockout (bottom) mice culled at ZT 0 and ZT 12. **Right**, Mean HCN4 protein expression determined by immunohistochemistry in the sinus node of control wild-type and cardiac-specific *Bmal1* knockout mice at ZT 0 and ZT 12 (wild-type mice, n=56/42 sections from 3/3 mice; cardiac-specific *Bmal1* knockout mice, n=38/46 sections from 3/3 mice). *P<0.05; two-way ANOVA with Holm-Šídák test. Same data as Figure 6F.

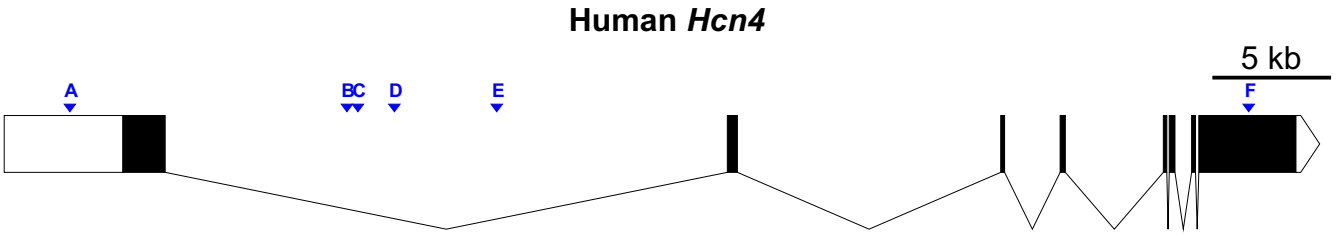

Supplemental Figure 3: Schematic representation of human *Hcn4* including 2 kb of its 5′ flanking region showing the position of six potential E-box binding sites (A-F) identified using Matinspector.